Journal of Materials Chemistry C

ROYAL SOCIETY OF CHEMISTRY

REVIEW

View Article Online
View Journal | View Issue

Check for updates

Cite this: J. Mater. Chem. C, 2025, 13, 6484

Advancements in surface plasmon resonance sensors for real-time detection of chemical analytes: sensing materials and applications

Sung Hwan Cho,†[a] Seungwon Choi,†[a] Jun Min Suh†[ab] and Ho Won Jang *[ac]

Received 19th November 2024,
Accepted 25th February 2025

DOI: 10.1039/d4tc04890c

rsc.li/materials-c

Chemicals are being used in various fields with the development of industry, but the importance of human safety from chemical exposure is becoming increasingly evident. Traditional detection methods, which analyze analytes through preprocessing, have limitations in real-time applications. In contrast, LSPR and SPR sensors, which can rapidly and accurately detect chemicals in real time, are among the most reliable methods for protecting against chemical threats. LSPR and SPR sensors detect minute interactions between sensing materials and chemicals through changes in absorbance and refractive index, enabling the accurate detection of even the smallest changes. To maximize the performance of LSPR and SPR sensors capable of real-time detection and apply them across various fields, ongoing research has focused on innovative materials, fabrication techniques, and nanostructures. The future perspectives on sensing materials for real-time detection technologies used by LSPR and SPR sensors are discussed. This review presents guidelines for selecting sensing materials for use in LSPR and SPR sensors in real-time applications.

Open Access Article. Published on 26 February 2025. Downloaded on 2/14/2026 10:12:37 AM.
This article is licensed under a Creative Commons Attribution-NonCommercial 3.0 Unported Licence.

1. Introduction

In modern society, the importance and versatility of chemicals in various industries, including biotechnology, semiconductors, and agriculture, are growing.[1,2] Additionally, as various compounds are newly synthesized or discovered, the types of chemicals used in modern society are increasing exponentially. However, with the development of these chemicals, concerns about the risks they pose—especially those that can have fatal effects on the human body even in small amounts—are also increasing.[3] For the continued development of humanity, coexistence with various types of chemicals is essential. Therefore, appropriate measures, such as early warning systems for chemicals emitted due to inadequate management, accidental damage, or improper disposal, are necessary.[4]

Developing accurate methods for detecting chemical risks is crucial for ensuring the safe use of chemicals. Various detection technologies have been developed, including inductively coupled plasma mass spectrometry (ICP-MS),[5] gas chromatography (GC),[6] and nuclear magnetic resonance (NMR).[7] However, existing methods have the disadvantages of being expensive and lacking real-time detection capabilities, which are essential for early risk detection. Real-time detection refers to a continuous and immediate monitoring process that provides instantaneous results or feedback as events unfold. It provides fast and accurate information about the presence of chemicals, even at extremely low levels, distinguishing it from traditional methods that need time-consuming laboratory analyses. The capacity to give rapid data is critical in emergency response scenarios, industrial settings, and environmental monitoring, ensuring efficient risk management.[8–10]

Sensor technology is a popular and promising detection method due to its advantages of excellent accessibility and the ability to detect chemicals in a relatively short period of time.[11,12] Sensors detect chemicals and transmit information through various methods, serving as an alarm to alert individuals to potential chemical threats. In addition to addressing chemical threats, constant monitoring of air, water, food, and daily products by sensors is required to gain a basic understanding of chemical exposures and ensure human safety.

Sensor technology has been developed in various forms to detect chemicals, including chemoresistive,[13] colorimetric,[14] field-effect transistor,[15] acoustic,[16] and plasmonic sensors.[17] In addition, sensors have made significant advances and play an important role in rapidly detecting very low concentrations of analytes. As a proactive safeguard, they allow for the identification, monitoring, and mitigation of possible risks to human

[a] Department of Materials Science and Engineering, Research Institute of Advanced Materials, Seoul National University, Seoul, 08826, Republic of Korea. E-mail: hwjang@snu.ac.kr
[b] School of Transdisciplinary Innovations, Seoul National University, Seoul 08826, Republic of Korea
[c] Advanced Institute of Convergence Technology, Seoul National University, Suwon 16229, Republic of Korea
† S. H. Cho, S. Choi, and J. M. Suh contributed equally to this work.

This journal is © The Royal Society of Chemistry 2025

Open Access Article. Published on 26 February 2025. Downloaded on 2/14/2026 10:12:37 AM. This article is licensed under a Creative Commons Attribution-NonCommercial 3.0 Unported Licence.

health, environmental sustainability, and industrial safety in our complex and chemically saturated modern society. Among the various sensor technologies, researchers have been actively focused on technologies capable of accurate and real-time detection, while localized surface plasmon resonance (LSPR) and surface plasmon resonance (SPR) sensors have been gaining significant attention because of their low-concentration detection limit, instantaneous detection, and exceptional adaptability.[18–20] The excellent sensing properties of LSPR sensors at the nanoscale allow them to detect minute amounts of target molecules at the ppb level, increasing the real-time validity of the detection results for trace amounts of hazardous substances.[21] Because LSPR sensors detect chemicals through changes in absorbance, they show a color change that can be easily confirmed even with a very small amount of analyte. Based on this easy accessibility, LSPR sensors do not require complex optical systems, making their miniaturization easier.[22] Furthermore, they can be integrated with microfluidics or lab-on-a-chip to construct compact systems.[23] This enables the development of small and portable sensing devices for real-time and on-site detection in diagnostics, food safety, and environmental monitoring. Alternatively, SPR sensors detect chemicals upon changes in refractive index through the adsorption of the sensing materials. Given that these detection methods are based on the real-time interaction of liquid or gas as it flows, they have the advantages of being able to measure even in flowing fluids.[24] Unlike LSPR sensors, they consist of bulky optical components for the accurate alignment of light, making it challenging to miniaturize them into simple devices.[22] Thus, to overcome this limitation, recent research has reported various approaches for miniaturizing SPR sensors, such as reducing the probe size by grating- or fiber-based SPR sensors that do not require prisms and optimizing the optical design by minimizing the size of optical components.[25,26] Furthermore, SPR sensors give crucial kinetic information, allowing researchers to confirm binding events and comprehend their temporal dynamics. Both LSPR and SPR show great promise for accurate real-time detection technology, promising breakthroughs in on-site monitoring and integration with emerging technologies, underlining their importance in the growth of analytical sciences.

The various advantages of LSRP and SPR sensors originate from the ability of sensing materials to respond to even the slightest interaction with chemicals, and thus they are widely used in both biological and non-biological domains. These properties are vital given that they allow selective interactions with the target analyte, ensuring that the sensor accurately and specifically responds to the desired substance. The tunability of the interactions that occur on the surface of the sensing material can improve both the specificity and sensitivity required for the detection of a wide range of chemicals, the development of which is continuously evolving. In the field of LSPR sensors, where the size and shape of nanoparticles are important, research is in progress through the shape of nanoparticles and the suitability of ligands, such as metal nanoparticles (NPs), bimetallic NPs, and metal–organic materials (MOMs). Alternatively, in the field of SPR sensors, where reactions with chemicals through adsorption are important, research is being conducted on materials that can be manufactured in the form of thin films, such as two-dimensional (2D) materials, metal oxides, and organic composites, as shown in Fig. 1.

The need for the development of LSPR and SPR sensors is increasing based on their wide applicability in bio and non-bio fields, and accordingly, research is being conducted on sensing materials suitable for each measurement method. In response to these emerging needs, active research is being conducted in LSPR and SPR sensors, as evidenced by the notable rise in the number of published papers and citations over the past decade, as shown in Fig. 2.

2. Principles of LSPR and SPR sensors

LSPR and SPR sensors have their roots in the broader fields of plasmonics and nanotechnology. The theoretical foundation for localized plasmons was presented by theorists including Mie in 1908, with early experimental work gaining momentum in the 1980s and 1990s.[27] The development of advanced nanofabrication techniques allowed precise control of the size and shape of NPs, influencing their sensing properties. In the late 1990s, researchers recognized the potential of LSPR and SPR for

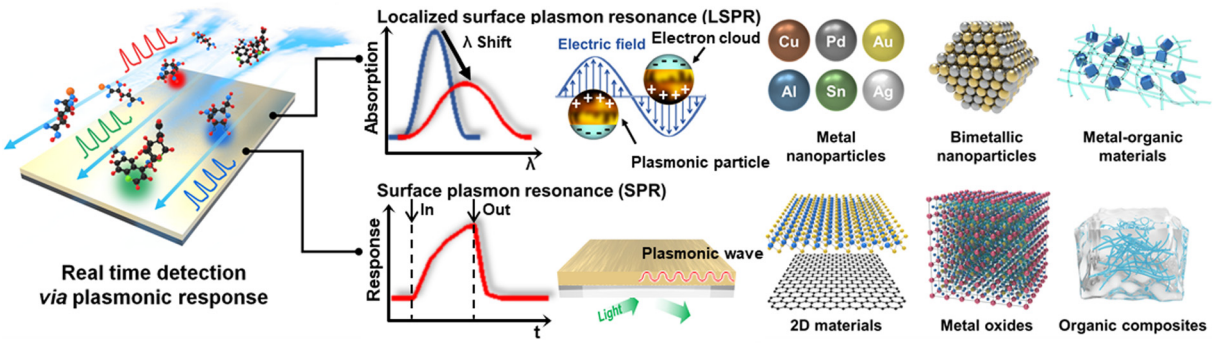

Fig. 1 Schematic of two representative technologies (LSPR and SPR) used in real-time detection *via* plasmonic reactions and the materials used for each technology.

Open Access Article. Published on 26 February 2025. Downloaded on 2/14/2026 10:12:37 AM.
This article is licensed under a Creative Commons Attribution-NonCommercial 3.0 Unported Licence.

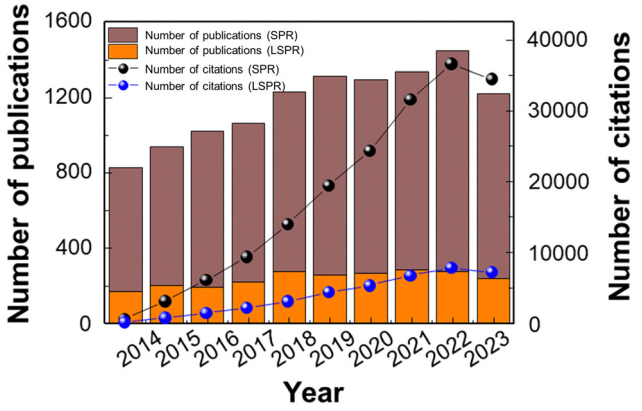

Fig. 2 Number of publications and citations on LSPR and SPR sensors. The data were collected using the Web of Science Core Collection, with the keywords "LSPR sensor" or "SPR sensor".

sensing applications due to their sensitivity to changes in the local environment.[28,29] This led to the introduction of LSPR- and SPR-based sensors, enabling real-time detection on the nanoscale.

The usage of LSPR and SPR sensors has evolved significantly over the years. LSPR sensors have found applications in diverse areas, ranging from biomedicine to environmental monitoring.[30,31] The unique optical properties of metal NPs in LSPR sensors allow the highly sensitive and selective detection of analytes at the nanoscale. In addition, research to improve their performance through material-based research based on metal NPs is continuing. Alternatively, SPR sensors, with the ability to monitor interactions of biomolecules and chemicals in real-time, have become indispensable in fields such as biochemistry, pharmaceuticals, and medical diagnostics.[32] The miniaturization and integration of SPR systems, together with advancements in SPR imaging techniques, have expanded their utility to portable and point-of-care applications. Ongoing research in both LSPR and SPR continues to explore new materials, configurations, and applications, promising further advancements in the field of optical sensing.

Surface plasmon refers to the collective oscillations of free electrons on the surface of metals, such as gold, silver, and copper. The electric field generated by surface plasmons at the metal–dielectric interface is called surface plasmon polariton (SPP), propagating along the interface and exponentially decaying away from the surface. When the size of a metal particle is comparable to the wavelength of light, the confined surface plasmon is referred to as localized surface plasmon (LSP). An absorption peak appears at the plasmon frequency of LSP (ω_{sp}) when irradiated in the visible and infrared range.[33]

$$\omega_{sp} = \sqrt{\frac{ne^2}{\varepsilon_0 m^*}} \Big/ \sqrt{1+\varepsilon_d}$$

where n is the electron density, e is the charge of an electron, ε_0 is the permittivity of free space, m^* is the effective mass of an electron, and ε_d is the dielectric constant of the dielectrics.

The position of this absorption peak depends on the size and shape of the metal NP, as well as the refractive index near its surface. When integrated into sensors, LSPR sensors operate by observing changes in absorption wavelength caused by the interaction between the analytes and the surface of NPs. This enhanced sensitivity to minute changes in NPs facilitates precise and real-time detection, positioning LSPR sensors as indispensable instruments in fields such as biotechnology, environmental monitoring, and medical diagnostics. A critical component in maximizing the sensing properties of LSPR-based sensors lies in material research, where investigations into metal NPs strive to tailor their size and shape for enhanced sensitivity and plasmonic effects. Bimetallic NPs offer a means for fine-tuning the LSPR characteristics, ensuring improved stability and durability, while MOMs introduce functionalization, amplifying the selectivity and enabling multifunctionality. This holistic approach to material research, encompassing metal NPs, bimetallic NPs, and MOMs, plays an important role in increasing the versatility and efficiency of LSPR sensors in a variety of applications ranging from biomedical diagnostics to environmental monitoring.

Alternatively, in SPR sensors, polarized light is irradiated on a nanometer-thick metal thin film at a specific incident angle and wavelength. The generated SPP on the metal film has a propagation constant (k_{sp}), which is calculated as follows:

$$k_{sp} = \sqrt{\frac{\omega}{c}\frac{\varepsilon_m \varepsilon_d}{\varepsilon_m + \varepsilon_d}}$$

where ε_m and ε_d are the dielectric constants of the metal and dielectrics, respectively, ω is the frequency of incident light, and c is the velocity of light.

When the propagation constant of SPP and the wavevector of incident polarized light are well matched, SPR occurs on the surface of the metal film.[34] The resonance angle and wavelength are sensitively influenced by changes in the refractive index near the metal surface. The adsorption of analytes induces a change in the refractive index near the metal surface and influences the resonance angle and wavelength. Thus, by tracking the resonance conditions, the interaction and kinetics between the analytes and sensing materials can be monitored sensitively in real-time. Accordingly, SPR sensors play an important role in applications such as drug discovery, medical diagnostics, and environmental monitoring due to their exceptional sensitivity and binding kinetics. Concurrently, research focused on the recognition layer, which is a thin functionalized sensing material on the sensor surface and responsible for adsorbing chemicals in SPR sensors, has proven to be indispensable for optimizing the performance of these sensors. Sensing materials in the recognition layer are being researched for their potential application in 2D materials such as graphene, which offer improved biocompatibility and high surface-to-volume ratio for enhanced sensitivity and real-time detection. Metal oxides improve the sensitivity and are valuable in applications such as environmental monitoring owing to their low cost and easy and versatile synthesis methods. Additionally, organic composites with customized functionalization are highly suitable for

 This journal is © The Royal Society of Chemistry 2025

Open Access Article. Published on 26 February 2025. Downloaded on 2/14/2026 10:12:37 AM. This article is licensed under a Creative Commons Attribution-NonCommercial 3.0 Unported Licence.

biomedical and chemical sensing due to their high selectivity, enabling the detection of the desired chemical. The ongoing investigation and refinement of material choices for the recognition layer constitute pivotal strides in advancing SPR sensors for a spectrum of applications, spanning medical diagnostics to environmental analysis.

3. Real-time monitoring properties of LSPR sensors

LSPR sensors offer distinct advantages for the real-time detection of chemicals over other technologies in terms of versatility and accuracy. The real-time monitoring capabilities of LSPR sensors allow continuous observation of chemicals to gain insight into the kinetics and affinity of the interaction between the sensing materials and chemicals. The low detection limit and great sensitivity of LSPR sensors are due to the characteristics of their sensing materials, which change their shape and size in response to even the slightest change, and with the development of optical measurement equipment, even minute changes in absorbance can be accurately measured. Additionally, LSPR sensors have the advantage of being able to detect chemicals with the naked eye without measuring equipment by detecting chemicals through changes in absorbance even with a small amount of sensing material. These various advantages improve the portability and applicability of LSPR sensors, allowing efficient, low-cost detection without restrictions in various fields where chemicals exist. Overall, the comprehensive attributes of LSPR sensors make them powerful tools for diverse applications in chemical sensing. The adaptability and versatility of LSPR sensors extend their utility across a wide range of applications, including biochemistry, environmental monitoring, medical diagnostics, and food safety. Thus, their wide applicability and ability to provide real-time information contribute to their widespread adoption in both research and industrial settings.

The advantages of LSPR sensors position them as valuable tools in the field of sensing, offering unique capabilities for precise, efficient, and real-time detection in chemical applications. Thus, diverse sensing materials are required to improve their sensing performance and real-time detection ability. Research is being actively conducted on metal NPs that most easily exhibit the LSRP phenomenon,[35–44] LSPR sensors with improved characteristics using various bimetallic NPs,[45–54] and the material-based LSPR sensors that show improved sensitivity by using organic particles in metal nanoparticles are summarized in Table 1.[55–60]

3.1 Metal NP-based LSPR sensor

Metal NP-based LSPR sensors are now widely used in sensing technology. The high surface-to-volume ratio and adjustable properties of these NPs, regulated by their form, make them ideal for immobilizing target molecules.[61,62] The exact geometry of metal NPs has a substantial impact on their plasmonic resonance frequencies, allowing fine tuning to meet the desired wavelength. Metal NPs exhibit a unique characteristic where their light absorption wavelength changes based on variations in their shape and size due to minuscule interactions with chemicals. This property enhances the sensitivity of LSPR sensors to environmental changes, resulting in superior detection capability

Table 1 Summary of LSPR sensors based on metal NPs, bimetallic NPs, and MOMs

Material type	Target type	Sensing materials[a]	Analyte	Detection range	Limit of detection	Ref.
Metal NPs	Bio	AuNRs	β-Galactosidase	0.1–10 nM	128 pM	35
		AgNPs	Melamine	0–10 μM	0.099 μM	36
		AgNPs	Timolol	0.1–1000 μM	1.2 μM	37
		AgNPs	Aflatoxin B1	1–10 ng mL^{-1}	0.36 ng mL^{-1}	38
		AgNPs	Cholic acid	0–30 μM	1 μM	39
		AgNPs	Omeprazole	0.05–40 μM	15 nM	40
	Non-bio	AuNRs	Cu^{2+}	0–1 mM	0.5 nM	41
		AgNPs	Cd^{2+}	1–10 μM	87 nM	42
		AgNPs	As^{3+}	5–500 μg L^{-1}	2 μg L^{-1}	43
		Ag NPR	Hg^{2+}	0.005–10 μM	0.2 nM	44
Bimetallic NPs	Bio	Ag/Au nanoshell	Glucose	0.002–2 mM		45
		Au nanocage	Gallic acid	0.01–5 μM		46
		Au nanocage	Vitamin C	0.05–7.5 μM	0.024 μM	47
		AuNRs	Ellagic acid	0.2–20 μM	0.04 μM	48
	Non-bio	GSH-s-Au/Ag nanoframe	Co^{2+}	1.7–17 μM	0.04 μM	49
		Pd/Au/Cu	H_2			50
		Au nanosphere/AgNRs	ClO^-	0.5–30 μM	0.24 μM	51
		Au/Ag nanocage	Hg^{2+}	0.03–35 μM	10 nM	52
		Au/Ag/AgCl core–shell NPs	NH_3	0–5000 μM	6.4 μM	53
		Ag/Cu NPs	Hg^{2+}	0.001–50 μM	0.51 nM	54
MOMs	Bio	Ag NPR/glucose oxidase	Glucose	0.2–100 μM	0.2 μM	55
		Sucrose capped AuNPs	Daclatasvir	0.01–1 μg ml^{-1}	0.008 μg ml^{-1}	56
		Amine/POSS-APBAs/AuNPs	Glucose	1–1000 μM	25 μM	57
	Non-bio	SA–AgNP/PVA nanocomposites	Hg^{2+}	0.9–1200 ppb	0.9 ppb	58
		AuNPs/PO-EGMA	Pb^{2+}	0.1–100 nM	25 pM	59
		Melamine–Au nanostars	Uric acid	0–100 μM	8.5 nM	60

Open Access Article. Published on 26 February 2025. Downloaded on 2/14/2026 10:12:37 AM. This article is licensed under a Creative Commons Attribution-NonCommercial 3.0 Unported Licence.

and precision. The adaptability of structuring metal NPs allows subtle control of the localized electromagnetic field, which affects the detection capabilities of LSPR sensors. With these considerations, LSPR sensors based on metal NPs, with their shape-dependent effects, have found significant use in biomedical diagnostics, environmental monitoring, and chemical sensing. This highlights their ability to provide high-performance and adaptable sensing technologies that meet the specific needs of various areas.

3.1.1 Biosensors applications. Among the LSPR sensors that detect through metal NPs of various shapes, Chen *et al.* reported research on detecting β-galactosidase (β-gal) using Au nanorods (NRs).[35] Real-time detection technology for β-gal is indispensable for uncovering the dynamics of gene expression, understanding cellular processes, capturing dynamic cell behaviors, and optimizing various biotechnological and medical applications. The real-time aspect enables a more nuanced and comprehensive analysis, providing researchers and practitioners with valuable insights into the temporal aspects of β-gal-mediated processes across different scientific domains.

The sensing mechanism described involves a multi-colorimetric assay using AuNRs and enzyme-induced metallization. In the absence of β-gal, the unhydrolyzed substrate, *p*-aminophenyl β-D-galactopyranoside (PAPG), cannot reduce Ag^+ to metallic Ag. As a result, the solution retains the initial color of the AuNRs, appearing light pink. However, in the presence of β-galactosidase, it cleaves PAPG into galactoside and a reducing agent (PAP). This reducing agent, in the presence of AuNRs, then reduces Ag^+ to metallic Ag. The reduced metallic Ag coats the surface of AuNRs, inducing a multicolor shift in the sample solution. Consequently, the color of the solution transitions from light-green to orange-red, correlating with the concentration of β-gal. This multi-colorimetric assay provides a visual indication of the presence of β-gal, allowing a qualitative and potentially quantitative assessment based on the observed color changes in real-time.

The researchers used the absorbance spectra to monitor the change in AuNRs in varying β-gal concentrations (Fig. 3(a)). As the concentration increased, the absorbance of the AuNRs increased and the wavelength absorbed decreased. A dynamic relationship between $\Delta\lambda_{max}$ and β-gal concentration was seen in the range of 0.1×10^{-9} to 10×10^{-9} M, as shown in Fig. 3(b). Fig. 3(b) demonstrates that the $\Delta\lambda_{max}$ value increased with an increase in the concentration of β-gal. As the concentration increased, the change in the wavelength decreased, but at low concentrations, the correlation between concentration and $\Delta\lambda_{max}$ was observed to be linear. This change in $\Delta\lambda_{max}$ could also be observed as a color change in the solution. As shown in Fig. 3(c), the detection solutions exhibited a color shift from light-green to orange-red compared to the control. The distinct multicolor changes at the concentration of 2.0×10^{-9} M could be easily identified visually. As shown in Fig. 3(d) and (e), the transmission electron microscopy (TEM) images showed that the synthesized AuNRs possessed a length of 59 ± 8 nm and width of 11 ± 1 nm. After, the reaction of the Ag shell on the body sides of AuNRs was observed. The deposition of an Ag shell on the

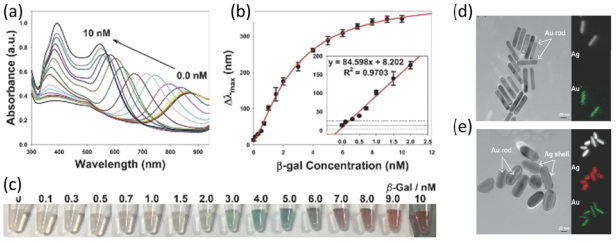

Fig. 3 (a) UV-vis absorption spectra and (b) the blue shift in the longitudinal LSPR peak of Au NRs in response to β-gal (0 to 10 nM). (c) Photographs of multi-colorimetric assays of AuNRs toward various concentrations of β-gal. TEM images of AuNRs (d) before and (e) after incubation with β-gal. Reproduced with permission from ref. 35 Copyright©2016, John Wiley & Sons.

surface of AuNRs was further investigated using high-resolution TEM-energy dispersive X-ray spectroscopy (EDS). The corresponding EDS Ag (red color) and Au (green color) mapping images also confirmed the coating of metallic silver on the surface of AuNRs. The Ag peaks in the EDS spectrum were observed after the enzyme-induced metallization. Both an enhancement in absorbance intensity and blue shift in the longitudinal LSPR peak were observed after the enzyme-induced Ag metallization on the surface of AuNRs. The longitudinal LSPR peak shifted from 885 to 520 nm, and the absorbance intensity of the longitudinal LSPR peak likewise increased with an increase in β-gal concentration.

3.1.2 Non-biosensor applications. Increased heavy metal exposure poses a major risk to human health. Heavy metals, including Pd, Hg, Cd, and As, are well-known for their toxic effects on the brain, kidneys, and other organs.[63,64] Prolonged exposure to high levels of these metals is linked to an increased risk of neurological issues, developmental abnormalities, renal damage, and some malignancies. This hazard is worsened by heavy metal bioaccumulation in the food chain, which allows toxic elements to be absorbed by plants and aquatic species before reaching human populations *via* polluted food and water. Thus, the current increase in the prevalence of heavy metal ions poses a major and far-reaching threat to the well-being of humans, needing immediate action to monitor, regulate, and minimize their influence on both human health and the environment. Many analysis methods have been developed to detect ions that have a very negative effect on the human body. However, although these approaches provide high sensitivity and multi-element analysis, they are costly, time consuming, complex, and challenging for on-site field testing. Alternatively, LSPR sensors not only possess the advantages of current detection technologies but also provide instantaneous detection. Their multiplexing property enables the simultaneous detection of numerous heavy metal ions, improving the analytical efficiency. The ability to design the characteristics of metal NPs in LSPR sensors allows their customization to specific heavy metal ions and sample circumstances. Owing to their minimal sample preparation requirements, portability, and potential for cost-effective analysis, LSPR sensors are well suited for on-site monitoring in a variety of settings, ranging from environmental monitoring to industrial applications,

 This journal is © The Royal Society of Chemistry 2025

Open Access Article. Published on 26 February 2025. Downloaded on 2/14/2026 10:12:37 AM. This article is licensed under a Creative Commons Attribution-NonCommercial 3.0 Unported Licence.

making them a valuable tool for addressing the critical challenges associated with heavy metal ion contamination.

Chen *et al.* reported the fabrication of an LSPR Hg^{2+} sensor based on the shape change of unmodified Ag nanoprisms (AgNPRs) by adding Hg^{2+} and $S_2O_3^{2-}$.[44] The proposed sensing mechanism in this study involves apical activation and passivation of triangular AgNPRs through the actions of $S_2O_3^{2-}$ and Hg^{2+}. $S_2O_3^{2-}$ acts as a leaching agent, rapidly truncating the sharp tips of unmodified AgNPRs into round nanodiscs, resulting in a distinct color change and a significant shift in the LSPR wavelength. This change is prevented in the presence of Hg^{2+}, which protects the AgNPRs from etching by forming HgS at their corner sites. Thus, the shape of the AgNPRs is frozen, allowing the quantification of Hg^{2+} ions in the solution, as shown in Fig. 4(a). The optical properties of the prepared AgNPR colloid, including a blue color and distinct LSPR absorption bands, were highly sensitive to trace reactions, controlling the edge length, thickness, and sharp tips of the AgNPRs. The sculpturing effect of $S_2O_3^{2-}$ and the passivation effect of Hg^{2+} were illustrated through changes in colloidal color and absorption spectra, as shown in Fig. 4(b). The addition of $S_2O_3^{2-}$ induced facet-selective etching reactions, leading to a blue to yellow color change and a blue-shift in the LSPR peak. In the presence of both $S_2O_3^{2-}$ and Hg^{2+}, the color change and LSPR shift are halted due to the formation of insoluble HgS at the tips of AgNPRs. The changes in the shape of individual AgNPRs in three separate cases were also verified *via* TEM analysis. TEM imaging revealed the original triangular shapes of AgNPR (Fig. 4(c)), circular nanodisc shapes in the presence of $S_2O_3^{-}$ (Fig. 4(d)), and additional angles in the presence of both $S_2O_3^{-}$ and Hg^{2+} (Fig. 4(e)).

Fig. 4(f) demonstrates that the reaction reached a steady state within 5 min, allowing quick detection and real-time detection. The concentration of Hg^{2+} can further tune the color change and LSPR wavelength, providing distinctive characteristics for wide-range Hg^{2+} detection within a short timeframe. The dominant interaction among AgNPR, $S_2O_3^{2-}$, and Hg^{2+} was identified as HgS deposition reactions within 5 min, contrasting with the longer etching reactions observed without $S_2O_3^{2-}$.

Metal NP-based LSPR sensors with a color shift due to agglomeration are dynamic and responsive sensing platforms. Metal NPs, often Au or Ag, are scattered in a solution to form these sensors. When exposed to specific analytes, the NPs aggregate, changing their spatial arrangement and causing a shift in the plasmonic resonance. This agglomeration-induced alteration appears as a distinct color shift in the solution, providing a visible readout. The color change mechanism provides an immediate and understandable indication of the presence and concentration of the target analytes, making these sensors ideal for applications requiring a quick and qualitative response. The issue of regulating agglomeration in these systems emphasizes the significance of careful design and optimization to improve the reliability and sensitivity of color-changing LSPR sensors in a variety of analytical and detecting applications.

3.2 Bimetallic NP-based LSPR sensors

Bimetallic NPs exhibit synergistic effects, where the interplay between the two metals influences their resonant frequency and nanostructure, resulting in an enhanced sensor performance. In addition to improved stability and durability, the distinctive characteristics of bimetallic materials, such as flexible morphological tunability, enable visual detection through multicolor changes and enhance the sensitivity and accuracy in LSPR sensing applications across diverse fields, including biomedical diagnostics, environmental monitoring, and chemical analysis.

3.2.1 Biosensor applications. He *et al.* utilized an Ag/Au bimetallic nanosphere (NS) glucose oxidase (GO_x) system to detect glucose by LSPR tehcnology.[45] The hollow and intact Ag/Au bimetallic NSs used as the sensing platform were synthesized using a colloid seed-engaged replacement reaction and a colloid-mediated deposition reaction, with hydroxylamine hydrochloride as a mild reducing agent. Subsequently, the Ag/Au–GO_x NS complex was generated *via* electrostatic adsorption of the negatively charged GO_x protein (PI = 4.2) onto the positively charged polyhistidine-coated NS surface at pH 6–7. During the procedure, an excess quantity of GO_x was employed to achieve monolayer saturation on the NS surface. As shown in Fig. 5(a), He's group reported the fabrication of an LSPR sensor based on the selective dissolution of Ag from the produced hollow Ag/Au bimetallic NSs by hydrogen peroxide, which was derived from the surface-confirmed enzymatic oxidation of glucose in the presence of oxygen. As the enzymatic H_2O_2 etching progressed, the surface plasmon band of the resulting porous NSs was gradually redshifted, reflecting the change in the concentration of hydrogen peroxide, which was a measure of the change in the concentration of glucose in the reaction system. The sensitivity of the sensor was believed to be increased by confining GO_x onto the surface of Ag/Au NSs by electrostatic adsorption.

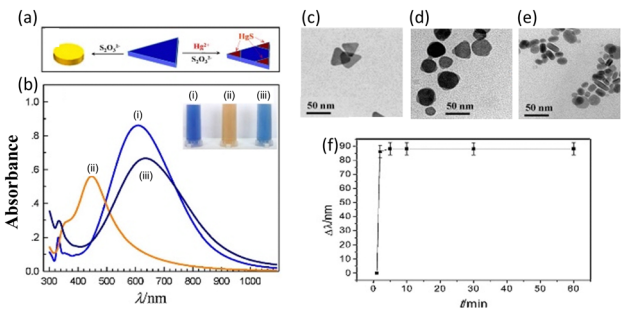

Fig. 4 (a) Schematic of the shape evolution of an AgNPR and growth of HgS in the presence of $S_2O_3^{2-}$ and Hg^{2+}. (b) UV-vis spectra and photographs (inset) of AgNPRs under 3 different conditions: (i) as-prepared, (ii) with $S_2O_3^{2-}$, and (iii) with $S_2O_3^{2-}$ and Hg^{2+}. TEM images of AgNPR: (c) as-prepared and with the addition of (d) $Na_2S_2O_3$ and (e) Hg^{2+} and $Na_2S_2O_3$. (f) Wavelength shift as a function of the reaction time for the AgNPR–Hg^{2+}–$Na_2S_2O_3$ mixture, pH 2.9. Reproduced with permission from ref. 44 Copyright©2015, Elsevier B. V.

Open Access Article. Published on 26 February 2025. Downloaded on 2/14/2026 10:12:37 AM. This article is licensed under a Creative Commons Attribution-NonCommercial 3.0 Unported Licence.

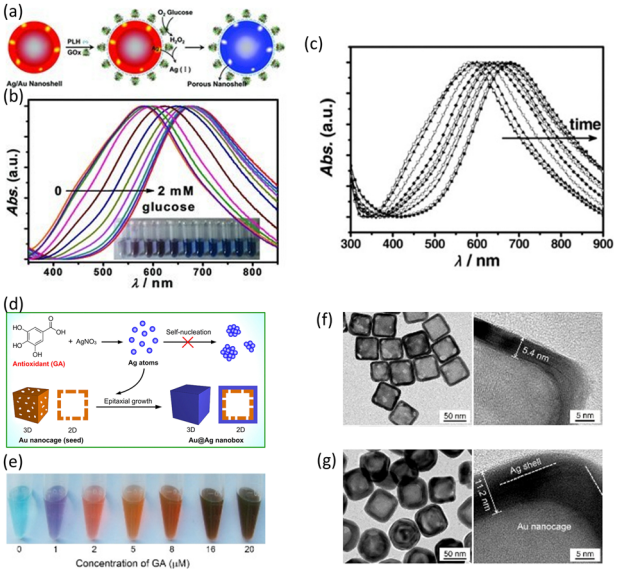

Fig. 5 (a) Process for the fabrication of Ag/Au bimetallic NSs and the sensing mechanism. (b) Normalized UV-vis extinction spectra of Ag/Au NSs after incubation with glucose in various concentrations (0 to 2 mM). (c) Time-dependent UV-vis absorption spectra of Ag/Au bimetallic NSs upon incubation with 3×10^{-3} M glucose. Reproduced with permission from ref. 45 Copyright©2012, John Wiley & Sons. (d) Schematic of the fabrication of Au/Ag nanoboxes. (e) Color changes in the creation of Au/Ag nanoboxes at various concentrations of gallic acid. TEM images of (f) Au nanocages in the absence of gallic acid and (g) Ag/Au nanoboxes in the presence of gallic acid. Reproduced with permission from ref. 46 Copyright©2018, Elsevier B. V.

Also, they investigated the sensitivity and applicability of the Ag/Au–GO_x NS system for optical glucose sensing. In this measurement, 1 mL aliquots of the as-prepared Ag/Au–GO_x NS suspension were incubated with 20 μL glucose solutions with a final concentration in the range of 0.002×10^{-3} to 2×10^{-3} M for 30 min. Fig. 5(b) shows a steady red-shift in the LSPR peak and a clear color change as the glucose concentration increased. A linear association was found between the LSPR peak shift of $\Delta\lambda_{max}$ and glucose concentration, ranging from approximately 0.5×10^{-6} M to 0.02×10^{-3} M.

Evaluating the real-time detection capability of a sensor can be effectively done by observing changes over a period of time. Fig. 5(c) displays the UV-vis spectra of the nanocomplex over time when incubated with a glucose concentration of 3×10^{-3} M. The λ_{max} of the nanocomplex progressively shifted to longer wavelengths when glucose was injected. After around 1–2 h, the shift leveled off and reached a saturation value. An observable transition in color, shifting from red-violet to blue, occurred within a time frame of 10 min. This implies that the Ag/Au–GO_x NS have the potential to be utilized for the practical colorimetric detection of glucose.

Nanostructures, with their small size and high surface-to-volume ratio, improve the sensing properties in a variety of applications.[13] The increased surface area of nanostructured materials creates more active sites, resulting in more significant interactions with the target analytes. The morphological change in Au nanocage to Au@Ag nanobox, and thus the LSPR evolution, was efficiently regulated by trace amounts of antioxidant, which acted as both a reductant in seed-mediated growth and a detecting target. Ag atoms can be produced through the redox reaction between Ag^+ and an antioxidant, such as gallic acid, as utilized in this study.[46] When Au nanocages (seeds) with a cubic shape, hollow interior, and numerous holes in their wall are present, newly generated Ag atoms deposit uniformly on the surface of the seeds by heterogeneous nucleation rather than self-nucleation. This results in the creation of Au@Ag nanoboxes with a hollow interior and closed wall (Fig. 5(d)). A new colorimetric approach for antioxidant assessment was devised using the morphological changes in nanoprobes and triggered LSPR evolution in the absence and presence of antioxidants.

This technique achieved high sensitivity *via* the heterogeneous nucleation of metal NPs, which requires a lower energy barrier compared to self-nucleation. Fig. 5(e) shows sample photographs of the color change of the solution at various gallic acid doses (0 to 20 μM). As the gallic acid content increased, the color changed from dark green to blue, red, orange, and brown.

The TEM images in Fig. 5(f) reveal hollow cubic Au nanocages with an outer edge length of 54.2 ± 3.5 nm and a wall thickness of 5.4 ± 0.8 nm. The pores on the side faces of the Au nanocages confirmed the characteristic nanocage morphology. In the presence of 4 μM gallic acid, the cubic nanocages were converted into nanoboxes with a hollow interior and closed walls. Compared to the original nanocages, the nanoboxes had significantly longer outer edges and thicker walls (Fig. 5(g)). The nanoboxes had an average size of 65.8 ± 5.3 nm, indicating an Ag layer of approximately 5.8 nm on the surface of the Au nanocages. The TEM images at a higher magnification revealed the outer layer of Ag and the contained nanocage due to the contrast between Au and Ag.

3.2.2 Non-biosensor applications. The primary focus of research on sensors utilizing plasmons has been on solution-based analytical technology, which relies on intense interactions with the analyte. Additionally, gas detection technology requires the selective detection of various unknown substances and stability to maintain the detection characteristics even in extreme environments because of poisoning effects.[65] Nevertheless, there is still a significant amount of research being done and a need for technology that can detect low concentrations of gases at room temperature selectively.[66] Among the various sensing materials, Pd is being investigated as a material for LSPR sensors due to its dual properties of significant catalytic activity for hydrogen production and plasmon resonance effect.[67]

Recently, Darmadi *et al.* demonstrated that a ternary PdAuCu alloy for plasmonic optical hydrogen detection could provide a solution to the poisoning effect.[50] Initially, they explored ternary PdAuCu nanoparticle arrays created using hole-mask colloidal lithography, which consisted of quasi-random configurations of nanodisks with an average diameter of 190 nm and a height of 25 nm (Fig. 6(a)). Au primarily contributes to the closure of the hysteresis gap, whereas Cu causes an elevation in the plateau region to higher hydrogen partial pressures. In the context of hydrogen sensors, the

 This journal is © The Royal Society of Chemistry 2025

Open Access Article. Published on 26 February 2025. Downloaded on 2/14/2026 10:12:37 AM. This article is licensed under a Creative Commons Attribution-NonCommercial 3.0 Unported Licence.

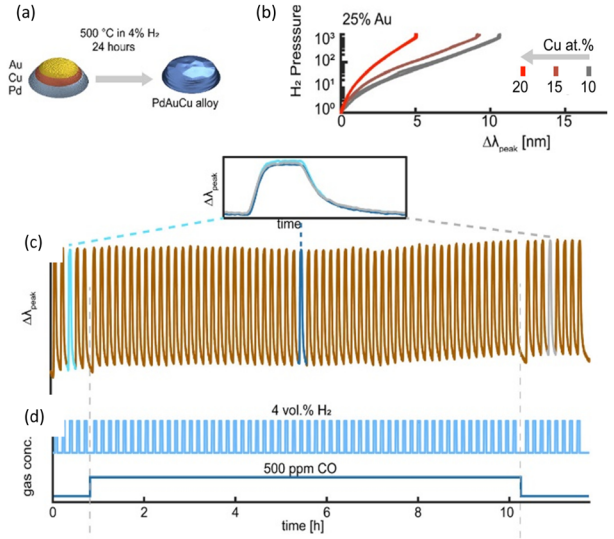

Fig. 6 (a) Schematic of the fabrication of PdAuCu alloy NPs. (b) Pressure-$\Delta\lambda_{peak}$ for PdAuCu ternary alloys with 25% Au concentration and 10%, 15%, 20% Cu content. (c) Temporal response of $\Delta\lambda_{peak}$ for the $Pd_{65}Au_{35}Cu_{10}$ alloy system to 4 vol% H_2 pulses in synthetic air at 30 °C. (d) Response with and without the 500 ppm CO background. Reproduced with permission from ref. 50 Copyright©2021, the American Chemical Society.

optimal ternary alloy composition is a balance between eliminating the hysteresis gap and maximizing the magnitude of $\Delta\lambda_{max}$ per hydrogen partial pressure change. Criterion (i) requires alloys with at least 25% Au, whereas criterion (ii) limits the Au and Cu concentrations, given that increasing them reduces the total sensor sensitivity due to the reduced peak per hydrogen partial pressure change. As a result of these selection criteria, the $Pd_{65}Au_{25}Cu_{10}$ ternary alloy system was identified as the best compromise, and hence the champion system. It is worth noting that the tiny gap between the absorption and desorption branches seen in Fig. 6(b) for the $Pd_{65}Au_{25}Cu_{10}$ alloy is a measurement artifact rather than an intrinsic hydride hysteresis gap. The absence of the α–β phase transition along the curve suggests hysteresis-free hydride production.

Darmadi's group investigated the resistance of $Pd_{65}Au_{25}Cu_{10}$ to poisoning, as shown in Fig. 6(c). They exposed it to over 50 pulses of 4% H_2 for 5 min each, while maintaining a steady background of 500 ppm CO, which is widely known to interfere with the reaction with hydrogen, in synthetic air carrier gas at a temperature of 30 °C.[68] This experiment lasted for 12 h, as shown in Fig. 6(d). The LSPR sensor exhibited remarkable stability and resistance to deactivation, as evidenced by its consistent response and recovery times throughout the experiment. Furthermore, the overall morphology and configuration of the nanodiscs on the surface remained unaltered even after the extended duration of the test.

Bimetallic NP-based LSPR sensors are a sophisticated type of sensing platform that exhibit the advantage of the synergistic features of two distinct metals, typically Au and Ag or Au and Cu. This metal combination allows greater tuning and control of the plasmonic sensing properties. Bimetallic NPs have distinct optical characteristics, which provide additional information for sensing applications. The different electrical and catalytic properties of each metal in the bimetallic framework help to improve the sensitivity and selectivity when detecting target analytes. These sensors have found applications in a variety of sectors, including environmental monitoring and biomedical diagnostics, where their customized composition enables their fine tuning for specific detection requirements. The use of bimetallic NPs in LSPR sensors demonstrates a diverse and advanced strategy that improves the capabilities of plasmonic sensing technologies for precise and reliable detection.

3.3 MOM-based LSPR sensors

MOMs have garnered attention for their unique properties in the context of LSPR sensors. MOMs are hybrid materials comprised of metal nodes interconnected by organic ligands, offering a diverse and tunable platform for LSPR applications. By incorporating various ligands into these structures, researchers can precisely control the properties of the resulting MOMs, influencing their electronic and optical characteristics. The surface functionalization of metal NPs provides selective binding sites and prevents the dissociation of metal NPs, leading to reversible measurements. This versatility allows the LSPR response to be tailored to specific applications, enhancing the sensitivity and selectivity of the sensor. The integration of MOMs in LSPR sensors with various ligands opens up possibilities for a wide range of functionalities, making them promising candidates for advanced sensing technologies in fields such as chemical analysis, environmental monitoring, and biomedical diagnostics.

3.3.1 Biosensors applications. Xia *et al.* present a simple but successful technique for the colorimetric imaging of glucose at the submicromolar level in blood utilizing unaltered Ag nanoprisms, with little theoretical complexity and physical requirements.[55] The sensing steps are shown in Fig. 7(a). Firstly, GO_x and Ag nanoprisms were simply combined, and then glucose was added to the homogenous mixture. Ultimately, the Ag triangle nanoprisms were etched to round nanodiscs by H_2O_2 created by enzymatic oxidation. The detection limit was 0.2 μM, which is lower than that of previously reported hybrid metal NP–GO_x systems. The exceptional sensitivity was attributed to (1) the extremely reactive edges/tips and (2) substantially tip sharpness and aspect ratio-dependent LSPR absorption of the Ag nanoprisms.

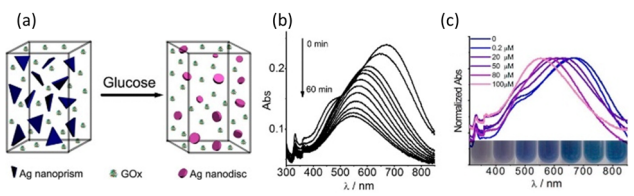

Fig. 7 (a) Schematic of the Ag–GO_x composite for glucose sensing. (b) Time-dependent LSRP absorption spectra of the Ag NPR upon incubation with 100 μM of glucose (0 to 60 min). (c) Normalized LSRP absorption spectra of Ag–GO_x at various concentrations of glucose (0 to 100 μM). Reproduced with permission from ref. 55 Copyright©2013, the American Chemical Society.

Open Access Article. Published on 26 February 2025. Downloaded on 2/14/2026 10:12:37 AM. This article is licensed under a Creative Commons Attribution-NonCommercial 3.0 Unported Licence.

The time-dependent LSPR bands of the homogeneous system that was exposed to a concentration of 0.1 mM glucose during incubation are shown in Fig. 7(b). The in-plane dipole band shift was observed to rapidly diminish within the first 10 min (90 nm), followed by a gradual decline until it reached a saturation value after around 30 min. The photograph of the LSPR sensor showed a steady blue shift in the in-plane dipole band and a clear color change in the Ag nanoplates (blue to purple to mauve) with an increase in glucose content, as shown in Fig. 7(c). This change in color is due to a change in the shape of Ag through the reaction. Due to its excellent sensitivity, only 10–20 μL of serum was sufficient for a single measurement. The proposed sensing device was extremely convenient, where the entire process, from Ag nanoprism creation to test completion, took less than an hour.

3.3.2 Non-biosensor applications. Subu *et al.* reported another MOM-based poly vinyl alcohol (SA–Ag/PVA) nanocomposite thin film for the detection of Hg^{2+}, which is one of the most fatal heavy metal ions to human beings.[58] Na-alginate reduced SA–Ag/PVA nanocomposite thin films were created *via* a simple synthetic technique. Rather than employing a functional monomer or cross-linking agent, they used sodium alginate, a biopolymer, for the imprinting process. The functional groups of this compound, including COOH, OH, and NH_2, allowed it to combine with Ag^+ (aq). After thermal activation, the OH functionality worked as a bio-reducing agent, converting Ag^+ to Ag. The resulting AgNPs were stabilized inside the sodium alginate network by various functional groups. The AgNP-imprinted sodium alginate network was converted into a nanocomposite thin film using polyvinyl alcohol (PVA), as shown in Fig. 8(a).

The functional groups containing oxygen in PVA have a binding affinity for Hg and Hg^{2+}, allowing them to diffuse into the nanocomposite film. Because the reduction potential of Hg^{2+}/Hg is higher than that of Ag^+/Ag, Ag is oxidized to Ag^+ and Hg^{2+} is reduced to Hg, forming an Ag/Hg amalgam and depositing Hg within the SA–Ag/PVA film simultaneously. This influenced the position and intensity of the LSPR peak for AgNPs within a few minutes. Fig. 8(b) exhibits the UV-vis spectra of the SA–Ag/PVA nanocomposite thin films immersed for 10 min in an aqueous solution with 1000 ppb of Hg^{2+} ions. Even after 2 min, the inclusion of Hg^{2+} caused a blue shift in the LSPR peak and decreased its intensity rapidly. The researchers also detected Hg^{2+} concentrations ranging from 2 to 1200 ppb and showed the good linearity of the absorption intensity, where the correlation coefficient was larger than 0.99. Furthermore, this sensor could detect Hg^{2+} concentrations ranging from 2 to 1200 ppb. The SA–Ag/PVA nanocomposite thin film sensor had computed LOD and LOQ values of 0.9 ppb and 3.07 ppb for Hg^{2+}, respectively.

An AuNP-poly(oligo-(ethylene glycol)methacrylate) (POEGMA) system was used to detect lead, which is classified as a major environmental pollutant due to its high toxicity.[59] Fig. 8(c) depicts the resultant sensing platform, which was developed using a detection chemical based on AuNP leaching. Firstly, AuNPs immobilized in POEGMA were functionalized with thiosulfate (by thiosulfate adsorption on AuNP surface).

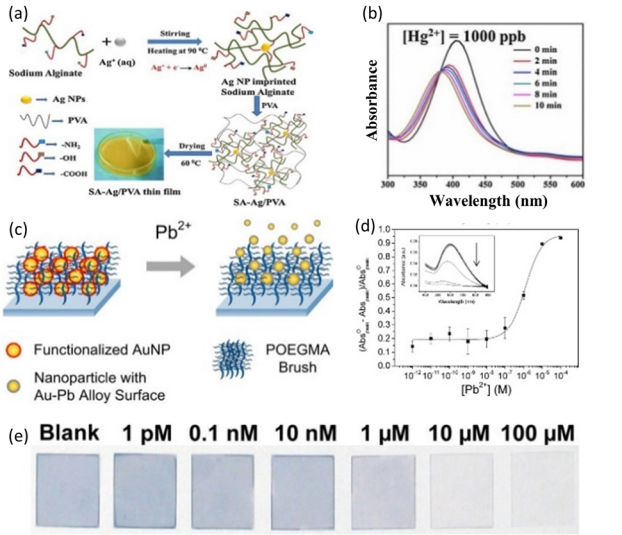

Fig. 8 (a) Schematic of the SA–Ag composite thin film for Hg^{2+} sensing. (b) LSPR peak of the SA–Ag composite in an aqueous solution of 1000 ppb of Hg^{2+}. Reproduced with permission from ref. 58 Copyright©2017, Elsevier B. V. (c) Pb^{2+} sensing mechanism of functionalized AuNPs. (d) Responses and (e) photograph to various concentrations of Pb^{2+} ranging from 1 pM to 100 μM. Reproduced with permission from ref. 59 Copyright©2013, the American Chemical Society.

The thiosulfate-functionalized AuNPs dissolved in the presence of 2-mercaptoethanol (2ME) and Pb^{2+} ions, forming an Au–Pb alloy on the AuNP surface and soluble Au^+–2ME complexes. The leached AuNPs with Au–Pb alloy on their surface no longer strongly interacted with the brush EG chains, allowing them to be released into solution. The AuNPs released from the POEGMA matrix reduced the UV-vis absorbance and color fading in the AuNP-POEGMA coated glass cover slip. This detection technique was chosen primarily because similar chemistry has been shown to detect lead with good sensitivity and specificity in solution. As a result, the performance in solution would be a useful baseline for comparison with solid-phase systems. Furthermore, unlike in-solution detection, which involves mixing thiosulfate and 2ME with the target and AuNPs in a single step, we were able to isolate the thiosulfate adsorption step here. This shows that preloaded AuNPs can be post-functionalized within the polymer brush using alternative detection techniques of interest. The detection capability of AuNPs in POEGMA was studied by immersing the substrates in water containing varying concentrations of Pb^{2+} from 1.00 pM to 100 μM in the presence of 2ME and calculating the reduction in absorbance, as shown in Fig. 8(d). Fig. 8(e) shows images of the AuNP-POEGMA samples after the detection of Pb^{2+}. The POEGMA-coated samples were easily identifiable by the naked eyes because of their high AuNP loading.

4. Real-time monitoring properties of SPR sensors

SPR sensors exhibit several advantages for the real-time detection of chemicals, distinguishing them from other detection

 This journal is © The Royal Society of Chemistry 2025

Open Access Article. Published on 26 February 2025. Downloaded on 2/14/2026 10:12:37 AM. This article is licensed under a Creative Commons Attribution-NonCommercial 3.0 Unported Licence.

technologies. A variety of analytes on the surface of metals can be sensed through adsorption on the sensing materials, allowing the detection of even minute levels in both liquid and gas. Also, SPR sensors are suitable for real-time measurement, given that they detect the interaction with chemicals in a fluid in motion. This simplifies experimental procedures, reduces potential interferences, and enables the direct and real-time observation of molecular binding events. SPR sensors excel in providing real-time kinetic data, offering insights into the association and dissociation rates of chemicals, which is crucial for understanding the dynamics of the interactions between chemicals and sensing materials. The high sensitivity of SPR sensors allows the detection of molecular interactions at low concentrations, making them particularly valuable for applications requiring the precise and quantitative analysis of chemicals.

SPR sensors have the advantage of being adaptable to a wide range of sensing materials that can selectively interact with the specific chemical being studied. SPR sensors possess high sensitivity, enabling the precise monitoring of molecule interactions even at low concentrations, down to the picomolar or femtomolar level. This adaptability applies to a range of sensing materials, allowing their modification based on the specific characteristics of the target chemical and enabling the immediate analysis of complicated materials, such as biological fluids. Additionally, SPR sensors are suitable for studying complex chemicals, offering a real-time approach to analyze the binding kinetics in their native environment. These attributes make SPR sensors powerful tools in chemical sensing, providing researchers and clinicians with a valuable platform for studying molecular interactions with high sensitivity, specificity, and real-time capabilities.

Various strategies can be employed to integrate these advantages with other detection techniques, depending on the type of sensing materials. Table 2 categorizes previously reported SPR sensors based on the types of sensing materials (2D materials,[69–78]

Table 2 Summary of SPR sensors based on 2D materials, metal oxides, and organic composites

Material type	Target type	Sensing materials[a]	Analyte	Detection range	Limit of Detection	Sensitivity	Ref.
2D materials	Bio	ADP3NSs	Amyloid-beta 1–42	1–10^4 pM	1 pM		69
		AuNPs/GeP_5NSs	SARS-CoV-2 RNA	10^{-2}–10^4 fM	10 aM	146° RIU^{-1}	70
		ssDNA/Cu-TCPP	Dopamine	5–5 × 10^5 pM	0.15 pM	2820.83 nm RIU^{-1}	71
		MoS_2NSs	Ferritin	50–400 ng mL^{-1}	Ferritin: 12 ng mL^{-1}	Ferritin: 0.024 nm (ng mL^{-1})$^{-1}$	72
		Ti_3C_2-MXene/AuNPs	Carcinoembryonic antigen	2 × 10^{-4}–2 × 10^4 pM	0.07 fM		73
		Peptide/Cu-TCPP NSs	Programmed death ligand-1 exosome	10^4–5 × 10^6 particles per mL	16.7 particles per mL	137.67° RIU^{-1}	74
		Graphene/Au	Glucose	0–300 mg dL^{-1}		3113 nm RIU^{-1}	75
		AuNRs-ssDNA/SbNSs	microRNA-21	10^{-2}–10^4 fM	10 aM	171° RIU^{-1}	76
	Non-bio	Graphene	2,4 Dinitrophenol	100–500 ppb	3 ppb		77
		Ti_2C-MXene NSs	Pb^{2+}	1–20 μg L^{-1}	79.2 ng L^{-1}	3.788 nm (μg L^{-1})$^{-1}$	78
Metal oxides	Bio	ZnO NPs/$MoSe_2$ NSs	Glucose	0–1.2 mg mL^{-1}	4.16 μg mL^{-1}	72.17 nm (mg mL^{-1})$^{-1}$	79
		Ta_2O_5NFs	Xanthine	0–3 μM	0.0127 μM	26.204 nm μM^{-1}	80
		Fe_3O_4	Glucose	0.1–10 mM	19.95 × 10^{-2} mM		81
		ZnO nanowires/CeO_2	Dopamine	10^{-3}–10 pM		95° RIU^{-1}	82
		ZnO	Neisseria meningitidis DNA	10–180 ng μL^{-1}	5 ng μL^{-1}	0.03° (ng μL^{-1})$^{-1}$	83
		Ta_2O_5 NPs embedded in rGO	Fenitrothion	0.25–4 μM	38.2 nM	24.02 nm μM^{-1}	84
	Non-bio	WO_3	NO_2	0.5–50 ppm			85
		NiO-doped ITO	H_2S	0.1–100 pm			86
		ZnO	CO	0.5–100 ppm	<500 ppb	0.091° ppm^{-1}	87
		$Fe_2H_2O_4$	As^{3+}	0.4–10 ppb	0.6 ppb	As^{3+}: 1.092° ppb^{-1}	88
Organic composites	Bio	AgNCs/chitosan	Mouse IgG	0.6–40 μg mL^{-1}			89
		MIP film	Histamine	25–10^3 μg L^{-1}	25 μg L^{-1}		90
		Triangular AgNPs/chitosan	Bovine IgG	7.5 × 10^{-2}–40 μg mL^{-1}	0.075 μg mL^{-1}		91
		Graphene/MIP film	L-Tryptophan	0.15–2.5 mM	0.105 mM		92
		AgNPs-CS-PSS-CS/GO	Beta-amyloid 1-42	2–4 × 10^8 fM	1.21 fg mL^{-1}		93
		Lipase/polyacrylamide gel	Triacylglyceride	0.5–7 mM		3.17 nm mM^{-1}	94
	Non-bio	MIP film	Profenofos	10^{-4}–10^{-1} μg L^{-1}	2.5 × 10^{-6} μg L^{-1}	12.7 nm (μg L^{-1})$^{-1}$	95
		GO/MIP film	Benzylpenicillin	1–100 ppb	0.021 ppb		96
		MIP film	Triclosan	0.05–1 ng mL^{-1}	0.017 ng mL^{-1}		97
		Pyrrole/chitosan/ITO	Cd^{2+}	0–200 μg L^{-1}	0.129 nM	1.306 nm (μg L^{-1})$^{-1}$	98

Open Access Article. Published on 26 February 2025. Downloaded on 2/14/2026 10:12:37 AM. This article is licensed under a Creative Commons Attribution-NonCommercial 3.0 Unported Licence.

metal oxides,[79–88] and organic composites.[89–98]) and analytes, and summarizes their performance.

4.1 2D material-based SPR sensors

2D materials are substances with layered structures such as graphene, transition metal dichalcogenides (TMDs), and MXenes. 2D materials have been gradually applied in chemical sensors due to their unique properties, such as large specific surface areas, optical properties, and photoelectric properties. The electron transport from 2D materials to Au films is facilitated by the lower work function of 2D materials in comparison to Au films when applied in SPR sensors.[99] The enhanced electron density on the Au film surface amplifies the plasmonic electric wave and the evanescent wave penetration depth. Because of its increased penetration depth, the SPR sensor responded more sensitively to changes in the refractive index of the sensing medium, leading to an increase in sensitivity. The large specific surface areas of 2D materials provide many reactive sites for interacting directly with target molecules. Furthermore, for the sensitive and selective detection of target molecules, a variety of receptors, such as antibodies, aptamers, and enzymes, is utilized. 2D materials can serve as immobilization layers for these receptors. These ultra-thin and uniform 2D materials exhibit a low damping effect given that they do not interfere with the plasmonic wave of metal films.[100] Ultimately, introducing 2D materials in SPR sensors enables selective and sensitive detection, resulting in fast response times, low cost, and simplicity to use, which are not shown by traditional techniques.

4.1.1 Biosensor applications. 2D materials utilizing substances produced within the body are widely employed in the field of biosensors. Biocomponents such as antibodies, aptamers, and enzymes recognize and bind to specific target molecules through interactions such as the specific binding of antigens and antibodies, the complementary base pairing of RNA and DNA, and protein–protein interactions. These biocomponents are immobilized on the large surface areas of 2D materials, binding selectively to specific target biomolecules even at low concentrations. The selective capture of biomolecules changes the refractive index around the sensing materials of SPR sensors, generating SPR signals. In addition to improving sensitivity through electron transport, these advantages of 2D materials can significantly enhance the performance of SPR sensors, enabling the selective and sensitive detection of biomolecules even at very low concentrations.

Owing to the rapid aging of the global population, the problems associated with aging are attracting increasing attention. Alzheimer's disease (AD) is one of the most common neurological disorders. To achieve its early diagnosis, the need for sensors that can distinguish between AD and amnestic mild cognitive impairment (aMCI) is rising. To diagnose AD, research is concentrating on sensors that can detect biomarkers, especially amyloid-beta 1–42 ($A\beta_{42}$). Gao *et al.* applied 2D biocomponents that can selectively bind to $A\beta_{42}$ to SPR sensors.[69] They detected $A\beta_{42}$ sensitively in the serum and plasma to distinguish between AD and aMCI through Alzheimer's disease

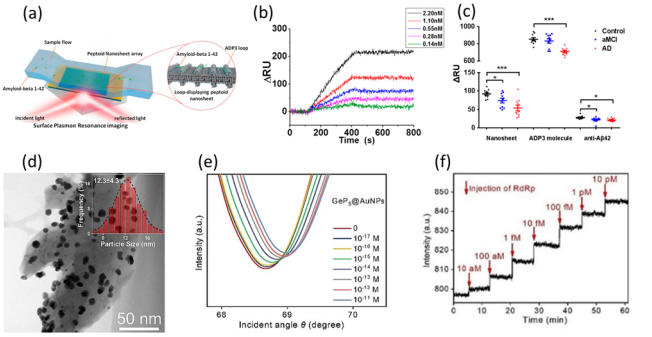

Fig. 9 (a) Schematic of the detection of $A\beta_{42}$ by ADP3NSs. (b) Real-time SPR responses for $A\beta_{42}$ at different concentrations ranging from 0.14 to 2.2 nM. (c) SPR responses for control individuals (n = 10), aMCI patients (n = 10), and AD patients (n = 10) using ADP3NSs, ADP3 molecules, and anti-$A\beta_{42}$. Reproduced with permission from ref. 69 Copyright©2020, the American Chemical Society. (d) TEM image of AuNPs-decorated GeP_5NSs (inset: the size distribution of AuNPs). (e) SPR spectra and (f) real-time SPR responses for RdRp at different concentrations ranging from 10^{-17} to 10^{-11} M. Reproduced with permission from ref. 70 Copyright©2023, Elsevier B. V.

peptoid 3 nanosheet (ADP3NS)-based SPR sensors. The amphiphilic peptoids have self-assembly characteristics through hydrophobic and electrostatic properties, making it easy to synthesize ordered ADP3NSs and form $A\beta_{42}$-binding loops on the surface. The surface-exposed loops on ADP3NSs function like the loops in an antibody that binds to a target antigen. To enhance the adsorption of $A\beta_{42}$ and restrict the nonspecific binding, Gao's group deposited uniformly distributed ADP3NSs on the surface of an Au layer and demonstrated the high sensitivity of the ADP3NS-based SPR sensor to $A\beta_{42}$ at the nM level, changing the refractive index near the sensing materials to further induce SPR signals (Fig. 9(a)). Fig. 9(b) shows the real-time SPR response to $A\beta_{42}$ in the concentration range of 0.14 to 2.20 nM. Significant signals were observed despite the extremely low concentration of $A\beta_{42}$. After about 300–400 s, the specific binding between the injected $A\beta_{42}$ and ADP3NSs reached dynamic equilibrium, where the response remained constant. Even at low concentrations of $A\beta_{42}$, it could be detected through specific binding with ADP3 and $A\beta_{42}$ in a rapid response time.

As shown in Fig. 9(c), $A\beta_{42}$ was detected in serum and plasma extracted from the blood of normal individuals (n = 10) and real patients with AD (n = 10) and aMCI (n = 10) based on different sensing materials, including ADP3NSs, ADP3 molecules, and anti-$A\beta_{42}$. In the case of these three sensing materials, it was observed that the MCI patients had lower signals than the normal individuals, whereas the AD patients had much lower signals, evaluating the ability of these sensors to distinguish between AD and aMCI and provide an accurate diagnosis. However, the difference in the signals among the groups was greatest in ADP3NSs, indicating that 2D ADP3NSs are most effective in distinguishing aMCI and AD. This research also demonstrated the outstanding sensitivity of ADP3NSs by showing a linear relationship between the SPR signals and $A\beta_{42}$ concentrations ranging from 1 pM to 10 000 pM. As a result, the authors demonstrated a highly sensitive and

Open Access Article. Published on 26 February 2025. Downloaded on 2/14/2026 10:12:37 AM. This article is licensed under a Creative Commons Attribution-NonCommercial 3.0 Unported Licence.

real-time SPR sensor capable of recognizing $A\beta_{42}$ at incredibly low $A\beta_{42}$ concentrations. The 2D ADP3NS SPR sensor can measure the concentration of $A\beta_{42}$ in the serum and plasma of real patients, and sensitively and accurately diagnose normal individuals, aMCI patients, and AD patients.

Covid-19, which emerged in 2019, rapidly spread worldwide, causing epidemic respiratory diseases and resulting in the immense loss of life. Due to the highly contagious nature of this virus, prompting the World Health Organization (WHO) to recommend self-isolation for infected individuals,[101] there was a crucial need for accurate and rapid diagnostics. Chang *et al.* introduced metallic 2D GeP_5NSs, which exhibited excellent electron transport properties upon contact with Au, decorated with AuNPs on an Au layer to detect SARS-CoV-2 RNA (RdRp).[70] In addition to enhancing the plasmonic wave by transporting electrons to the Au film, GeP_5NSs significantly improved the sensitivity of the sensor by strengthening the coupling between the SPR of the Au film and the LSPR of AuNPs. Also, AuNPs immobilized complementary RdRp (cRdRp), which hybridized with RdRp. When RdRp is injected, the cRdRp on AuNPs captures RdRp, causing fluctuations in the refractive index around the sensing materials. Then, GeP_5 and AuNPs amplify the SPR signals, leading to highly sensitive detection. Chang's group successfully assembled GeP_5NSs on an Au film *via* the layer-by-layer technique and decorated the NSs with AuNPs facilely to assist the sensitivity enhancement. As shown in Fig. 9(d), the TEM image confirmed the presence of uniformly distributed AuNPs on GeP_5NSs and the inset presenting the size distribution of AuNPs shows that the average size of AuNPs is 12.3 ± 4.3 nm.

The SPR spectra for various concentrations of RdRp ranging from 10^{-17} to 10^{-11} M are shown in Fig. 9(e). In the SPR spectra, the reflectance curves shifted upward and to the right as the concentration of RdRp increased. The significant increase in resonance angle and minimum reflectance was caused by the hybridization of the injected RdRp with cRdRp. The ability to exhibit linearity across an extensive range and produce a meaningful response even at a very low concentration of 1 pM showed the high sensitivity of this sensor for detecting RdRp. Fig. 9(f) demonstrates that the proposed AuNP/GeP_5NS SPR sensor can be applied for the real-time monitoring for RdRp. This sensor showed a linear and real-time increase in response as the concentration of RdRp continuously increased. Moreover, the sensor reached dynamic equilibrium within several minutes for each detection, and the time taken to reach equilibrium was consistent across all concentrations. Thus, this ultrasensitive, real-time, and rapid SPR sensor, which showed a noticeable performance, is applicable for detecting RdRp and diagnosing Covid-19.

2D materials can enhance the electron density on plasmonic metals and further improve the plasmonic electric field, leading to an enhancement in sensitivity. Also, the large surface area of 2D materials provides abundant active binding sites based on the immobilization of biocomponents. As a result, the sensitivity and selectivity of SPR sensors are dramatically enhanced. 2D materials offer the potential to be applied in practical applications such as pharmaceutical research and disease diagnosis using SPR biosensors.

4.1.2 Non-biosensor applications. Graphene and its derivatives, such as graphene oxide (GO) and reduced graphene oxide (rGO), are 2D materials that have large surface areas and superior physical and chemical properties compared to traditional materials such as oxides and nitrides. Graphene, composed of a single layer of carbon rings, can adsorb chemical molecules containing aromatic rings through pi–pi stacking. Also, GO and rGO possess many functional groups, such as hydroxyl groups and ester groups, which allow them to form pi–pi stacking and hydrogen bonds with various chemicals. The large surface area of graphene, GO, and rGO maximizes the active sites to interact with chemical substances such as small dye molecules, antibiotics, and pesticides. Due to these properties, label-free and real-time 2D material-based SPR sensors can detect chemical molecules sensitively and be utilized in studying the kinetics of binding.

Isopropyl alcohol (IPA) is a solvent used for cleaning in semiconductor processing technology. Thus, maintaining a high purity of IPA is critical for increasing the overall yield of semiconductor manufacturing processes.[102] Cho *et al.* reported the fabrication of a graphene-based SPR sensor that can detect 2,4-dinitrophenol (2,4-DNP), one of the aromatic compounds that may dissolve in IPA.[77] Fig. 10(a) illustrates the SPR

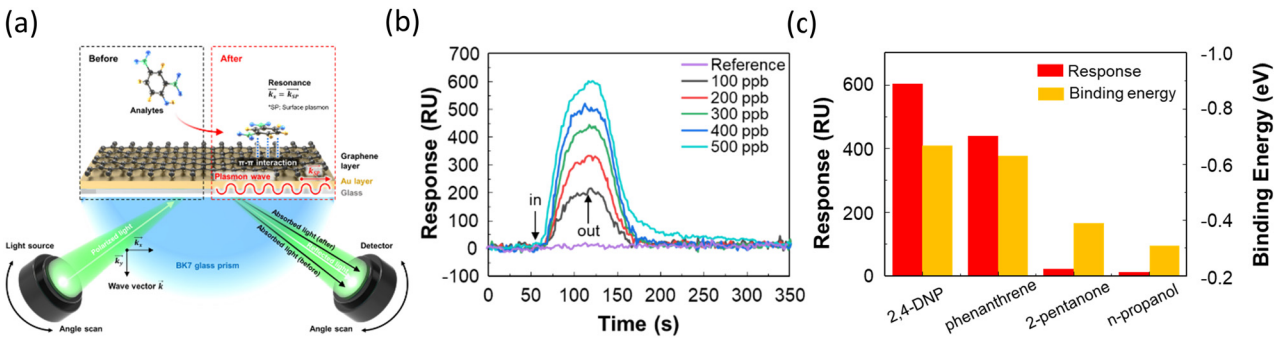

Fig. 10 (a) Schematic of the detection of 2,4DNP on a graphene-based SPR sensor. (b) Real-time SPR responses for 2,4 DNP at different concentrations ranging from 100 to 500 ppb. (c) Responses and calculated binding energies for various impurities. Reproduced with permission from ref. 77 Copyright©2024, John Wiley & Sons.

Open Access Article. Published on 26 February 2025. Downloaded on 2/14/2026 10:12:37 AM. This article is licensed under a Creative Commons Attribution-NonCommercial 3.0 Unported Licence.

measurement system, where 2,4-DNP interacts with the recognition layer, graphene. SPR signals are produced by the adsorption/desorption of 2,4-DNP on graphene through pi–pi stacking, which induces fluctuations in the local refractive index on the Au film. The authors demonstrated that 2,4-DNP, containing electron-withdrawing NO_2 groups, adsorbs on graphene by pi–pi stacking, causing p-doping in graphene. The shift in the transfer curve of solution-gated field-effect transistors and the peak shift in Raman spectra were used as evidence of this p-doping effect.[103,104] The real-time detection of 2,4-DNP was shown in the concentration range of 100 to 500 ppb (Fig. 10(b)). Even at very low concentrations of several hundred ppb, the SPR sensor exhibited substantial responses and outstanding quick response time and recovery time of 31 and 38 s, respectively. Other aromatic and non-aromatic compounds were detected by this SPR sensor at 500 ppb. The aromatic compound phenanthrene, which can strongly interact with graphene through pi–pi stacking, showed a high response, while two non-aromatic compounds, 2-pentanone and *n*-propanol, exhibited no significant responses (Fig. 10(c)). The binding energies calculated by density functional theory confirmed a similar trend to these results.

Owing to their substantial surface area and remarkable electrical and optical properties, 2D materials exhibit strong and sensitive binding with chemical substances.[105] In particular, graphene and its derivatives, composed of carbon rings in an extensively large surface area, can effectively interact with chemical molecules containing aromatic rings, maximizing the pi–pi stacking. This enables graphene and its derivatives to efficiently adsorb various molecules and produce SPR signals. The ability to enhance the plasmonic electric wave and maximize the binding with chemical molecules enables the use of 2D materials for the real-time detection of chemical molecules *via* SPR sensors and the observation of the kinetic binding between 2D materials and chemical molecules. The combination of 2D materials and SPR holds broad applications in environmental monitoring, food monitoring, and chemical analysis.

4.2 Metal oxide-based SPR sensors

In recent years, metal oxides have attracted significant interest in the field of bio-chemical sensors, owing to their biocompatibility, low-cost, and facile synthesis. Their versatility enables the development of composites containing 2D materials and organic materials, as well as the fabrication of diverse nanostructures. Metal oxides, when incorporated into SPR sensors, exhibit multifunctionality, including enhancing sensitivity, immobilizing biocomponents, and directly binding with target molecules. Metal oxides applied in guided wave surface plasmon resonance can strengthen the plasmonic wave and improve the sensitivity of the sensor when deposited very thinly on plasmonic metals due to their high refractive index.[106] Additionally, metal oxides can directly interact with target molecules through intrinsic oxygen vacancies or electron transfer. Also, they can immobilize biocomponents that selectively bind to target molecules. The binding of target molecules to metal oxides or biocomponents on metal oxides induces changes in the refractive index around the sensing materials, resulting in the generation of SPR signals.

4.2.1 Biosensor applications. Various biomarkers, including neurotransmitters, hormones, and metabolites, can be detected by several analyses to diagnose diseases. However, the traditional methods that have been researched for the selective detection of biomarkers have critical limitations. For example, fluorescent sensors require labeling target molecules, and liquid chromatography is time consuming for detection.[107,108] Thus, research is actively underway on real-time SPR sensors, enhanced by the deposition of metal oxides to improve the sensitivity and selectivity for the detection of target molecules.

Among the metabolites, xanthine is one of the intermediate compounds occurring during the metabolism of purine nucleotides. Given that xanthine is converted into uric acid by the xanthine oxidase (XO) enzyme, the concentration of xanthine serves as an indicator for pathological diseases such as gout, hyperuricemia, cerebral ischemia, perinatal, and tumor hyperthermia.[109] Kant *et al.* reported the fabrication of a sensitive and selective SPR sensor for xanthine by depositing Ta_2O_5 nanofibers (Ta_2O_5NFs) and immobilizing XO enzyme on a Ag layer (Fig. 11(a)).[80] They enhanced the plasmonic wave and further improved the sensing performance by depositing a thin film of high refractive index Ta_2O_5 NFs on an Ag film. Additionally, they immobilized XO enzymes on the surface of the sensing material, selectively decomposing only xanthine and inducing changes in the refractive index around the sensing material. The combination of these two effects resulted in the development of a highly sensitive and selective sensor for xanthine.

As shown in Fig. 11(b), to validate the selectivity of the XO enzyme, three interferents were compared with respect to shifts in the resonance wavelength. Interferents such as caffeine, glucose, and ascorbic acid showed negligible shifts of less than 10 nm, whereas xanthine showed a significant shift of over 40 nm. The specific recognition and decomposition of enzymes are suitable for application in SPR sensors for sensitive and selective detection. Fig. 11(c) illustrates the real-time SPR response of the XO/Ta_2O_5-based sensor. The change in the transmission intensity (λ = 617.5 nm) before and after the injection of 3 μM xanthine clearly shows that the response decreased and saturated within one minute after the injection. Furthermore, the response recovered to its original value and remained steady one minute after xanthine was removed. This indicated that both the response time and recovery time are less than one minute, implying that the proposed SPR sensor is very fast and can detect in real time.

Kant *et al.* improved the sensing performance by depositing a high refractive index metal oxide, enhancing the plasmonic electric wave. They also immobilized an enzyme on a metal oxide. As a result, the sensitivity and selectivity of the sensor were remarkable, and its rapid response time and recovery time make it highly suitable for practical application in disease diagnosis.

One of the most significant indicators of health management is glucose, which is especially relevant for diabetes. The real-time

 This journal is © The Royal Society of Chemistry 2025

Open Access Article. Published on 26 February 2025. Downloaded on 2/14/2026 10:12:37 AM.
This article is licensed under a Creative Commons Attribution-NonCommercial 3.0 Unported Licence.

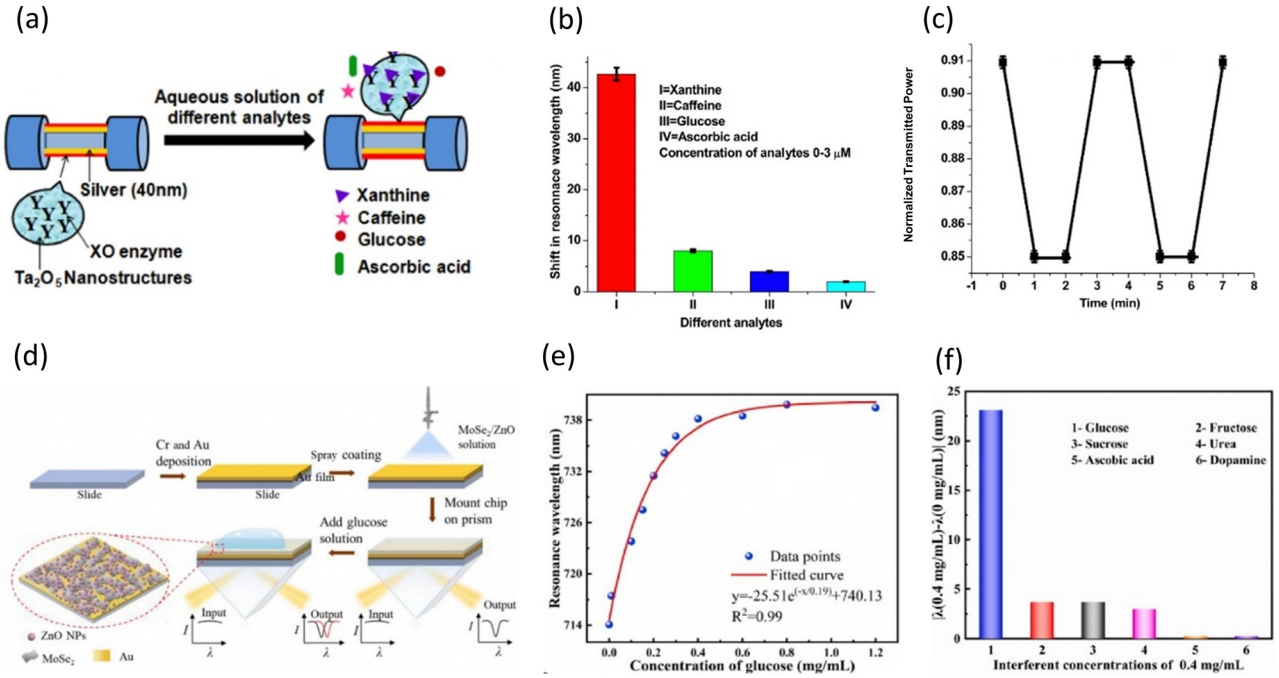

Fig. 11 (a) Schematic of the detection of xanthine on an XO enzyme-entrapped Ta_2O_5 NF-based SPR sensor. (b) Resonance wavelength shifts compared with interferents. (c) Real-time SPR responses for 3 μM xanthine. Reproduced with permission from ref. 80 Copyright©2017, Elsevier B.V. (d) Schematic of the fabrication of $MoSe_2$/ZnO-based SPR chips. (e) Resonance wavelength shifts for glucose at different concentrations ranging from 0 to 1.2 mg mL^{-1}. (f) Selectivity analysis with 0.4 mg mL^{-1} interferents. Reproduced with permission from ref. 79 Copyright©2023, Elsevier B.V.

measurement of blood glucose levels is necessary for maintaining the blood glucose levels within the normal range and diagnosing diabetes.[110] Besides diabetes care, medical and biological research,[111] food monitoring,[112] and systematic training for athletes[113] are all greatly correlated with the prompt and accurate detection of glucose. Chen *et al.* introduced a ZnO NP/$MoSe_2$ NS composite film in an SPR sensor for the detection of glucose without utilizing enzymes.[79] Fig. 11(d) illustrates the simple procedure for preparing the non-enzymatic ZnONP/$MoSe_2$ NS-based sensor. The sensor chip was fabricated by spray coating a ZnO NP/$MoSe_2$ NSs composite solution onto an Au film. The ZnO NPs in the sensing layer can bind to glucose through chemisorption on their surface, inducing fluctuations in the refractive index. Furthermore, ZnONPs can easily form composites with $MoSe_2$ NSs, which have large surface areas and outstanding electrical properties. This can be achieved by simply dissolving them in an organic solvent and heating. The composite film of ZnO NPs and $MoSe_2$ NSs recognized and bound to glucose sensitively and selectively without enzymes and amplified the signals.

Employing the non-enzymatic ZnO NP/$MoSe_2$ NS-based sensor, the authors detected glucose in the concentration range of 0 to 1.2 mg mL^{-1} (Fig. 11(e)). Under the optimized conditions, this sensor exhibited a total wavelength shift of 25.75 nm for glucose in the range of 0 to 1.2 mg mL^{-1}. Furthermore, this optimized sensor demonstrated linearity within the range of 0 to 0.3 mg mL^{-1}, sensitivity of 72.17 nm (mg mL^{-1-1}), and calculated limit of detection (LOD) of 0.023 mM. This highly sensitive performance is comparable to that of previously reported enzyme-based sensors. Because of their similar structures and properties to glucose, fructose, sucrose, urea, ascorbic acid, and dopamine are significant interferents in actual glucose detection applications. Fig. 11(f) illustrates the resonance wavelength shifts for the interferents and glucose at 0.4 mg mL^{-1}. The resonance wavelength shifts for fructose, sucrose, and urea were 3.75 nm, 3.8 nm, and 2.41 nm, respectively. Also, the shifts for ascorbic acid and dopamine were less than 1 nm. All these shifts were negligible in comparison to the large shift generated by glucose, indicating the excellent selectivity of the non-enzymatic ZnO NPs/$MoSe_2$ NS-based sensor.

A highly sensitive and selective ZnO/$MoSe_2$-based glucose sensor without enzymes was reported by Chen's group. ZnO NPs bind to glucose, and $MoSe_2$ NSs enhanced the sensitivity of the sensor. With an LOD of 0.023 mM and sensitivity of 72.17 nm $(mg\ mL^{-1})^{-1}$ in the linear range of 0 to 0.3 mg mL^{-1}, the sensor performed excellently not only in detecting glucose but also exhibited good selectivity against five interferents. Owing to its performance, this sensor has potential to be applied as a biosensor in medical diagnostics, bio-medical research, and food monitoring.

Depositing a thin layer of high refractive index metal oxide onto a plasmonic metal can enhance the plasmonic wave, thereby improving the sensing performance. Additionally, the characteristics of metal oxides, such as their ability to form composites easily with other substances, together with their intrinsic features such as oxygen vacancies and electron transfer for direct interaction with target substances, contribute to enhancing the binding with target molecules. Owing to these

Open Access Article. Published on 26 February 2025. Downloaded on 2/14/2026 10:12:37 AM. This article is licensed under a Creative Commons Attribution-NonCommercial 3.0 Unported Licence.

effects, metal oxide-based SPR sensors can rapidly, sensitively, and selectively capture target molecules. These sensors are expected to find widespread use in fields demanding highly sensitive, label-free, and real-time sensing capabilities, such as healthcare devices and medical research.

4.2.2 Non-biosensor applications. Metal oxides, particularly WO_3, SnO_2, and TiO_2, are extensively used in the field of gas sensors.[66,114–116] These metal oxides interact with toxic gases such as hydrogen, acetone, ammonia, and NO_2, enabling their detection. Numerous studies have shed light on the interaction between gas molecules and metal oxides such as chemisorption. Therefore, metal oxides can be applied in SPR sensors, allowing the real-time and highly sensitive detection of gas molecules, even at very low concentrations.

Among the toxic gases, NO_2 is a serious air pollution gas that can cause significant health issues in humans.[117] Thus, in the last few decades, various sensors have been developed to detect NO_2, including colorimetric sensors,[118] chemoresistive sensors,[119] and surface acoustic sensors.[120] However, all these sensors have certain shortcomings, such as low sensitivity, excessive power consumption, and sluggish response time. Alternatively, because of the high sensitivity, low power consumption and fast response time of SPR sensors incorporating metal oxides, they have become a promising technology for NO_2 detection. Most importantly, metal oxide-based SPR sensors are particularly suitable for applications such as industrial safety monitoring and environmental monitoring, where the real-time detection of hazardous gases such as NO_2 at room temperature is critical. This has led to ongoing research on SPR sensors for accurate and efficient NO_2 monitoring in various environments. Paliwal *et al.* proposed an SPR sensor with a WO_3 thin film as the sensing material for NO_2 detection at room temperature.[85] Considering the properties of SPR sensors where gas detection occurs on the sensor surface, a WO_3 film was deposited onto an Au layer through RF-magnetron sputtering at different growth pressures to control the grain boundaries and surface roughness. Fig. 12(a) illustrates the SPR gas sensing measurement. They suggested the mechanism for NO_2 detection based on the change in the refractive index of WO_3 due to the adsorption of NO_2. The mechanism is related to the refractive index changes of WO_3 based on the adsorption of NO_2. As an oxidizing gas, NO_2 takes electrons from WO_3, forming either NO_2^-, NO, or O^-, and then NO_2^- and O^- adsorb on the surface of WO_3. The refractive index of WO_3 changes as a result of electron loss and the adsorption of NO_2^- and O^-, leading to the generation of an SPR signal.

Fig. 12(b) shows the SPR spectra at different concentrations of NO_2 from 0 to 250 ppm for the sensor fabricated under the optimized condition. As the concentration of NO_2 increased, it was found that the resonance angle and the minimum reflectance increased, and the curves became broader. The huge shift in resonance angle with concentration indicates that the above-mentioned mechanism is valid. Furthermore, the significant changes in resonance angle and minimum reflectance demonstrate that this sensor is highly sensitive and effective for NO_2 detection. The pink curve in Fig. 12(c) represents the real-time SPR responses based on the reflectance changes of the sensor fabricated under the optimized condition. The responses saturated in less than 2 s when NO_2 was injected for every measured concentration. As air was reinjected for recovery, the responses also returned to their original values within 2 s. The rapid response and recovery times achieved when detecting at room temperature were notably fast and comparable to or even faster than traditional methods measured at elevated temperatures. These advantages make the WO_3-based SPR sensor highly suitable for real world application, where the rapid detection of hazardous gases is essential. Furthermore, after the repetitive detection of NO_2, there was no discernible change in the baseline. All these results confirm the high sensitivity of the WO_3-based SPR sensor reported by Paliwal's group, together with its very fast response and recovery time, real-time detection capability, and good stability, which are attributed to the physical and chemical adsorption of NO_2, withdrawing electrons from WO_3.

Metal oxides are inexpensive, easy to form nanostructures, and can synergize with other materials, making them suitable for the detection of chemical substances such as gas molecules in SPR sensors. Metal oxides can adsorb chemical molecules physically and chemically either through their intrinsic oxygen vacancies or direct electron transfer. Compared to previously reported sensors, metal oxide-based SPR sensors exhibit significantly faster response and recovery times, together with higher sensitivity. Furthermore, metal oxide-based SPR sensors have exceptional properties for repeatability and long-term stability due to the inherent stability of metal oxides. As a result, metal oxide-based SPR sensors can be widely applied in the fields of industrial safety monitoring, environmental monitoring, and water quality management.

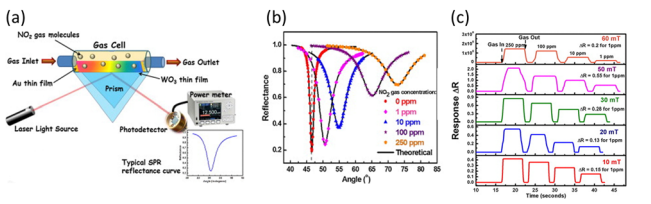

Fig. 12 (a) Schematic of the SPR gas sensing measurement. (b) SPR spectra for NO_2 gas at different concentrations ranging from 0 to 250 ppm. (c) Real-time SPR responses for sensors with WO_3 thin films grown at different pressures, with repetitive exposure to NO_2 gas at different concentrations ranging from 1 to 250 ppm. Reproduced with permission from ref. 85 Copyright©2015, Elsevier B.V.

4.3 Organic composite-based SPR sensors

Organic composites refer to materials formed by the combination of organic molecules, which are composed of carbon skeletons and other elements such as H, O, and N, with other substances such as other organic molecules, metals, metal oxides, and nitrides. Organic composites are employed in constructing sensing materials to uniformly distribute metal NPs and reactive materials that interact with target molecules to enhance the plasmonic electric field and increase the number of active sites. Additionally, organic composites are

Open Access Article. Published on 26 February 2025. Downloaded on 2/14/2026 10:12:37 AM. This article is licensed under a Creative Commons Attribution-NonCommercial 3.0 Unported Licence.

also utilized in the formation of molecular imprinting polymer (MIP) films, which provide specific binding sites for target molecules. The MIP film method is a technique for forming sensing materials by mixing and polymerizing target molecules with other organic molecules. After depositing a uniform polymer film, the target molecules are eliminated, creating imprinted sites on the surface of the sensing material. The created vacant sites can only adsorb the target molecules highly selectively and sensitively, leading to a fluctuation in the refractive index around the sensing material and generation of SPR signals. Due to these capabilities, researchers have employed many organic composites for composing sensing materials in the fields of environmental monitoring, biomedical research, and biosensors.

4.3.1 Biosensor applications. Organic composites can be synthesized by simply mixing various substances, including organic molecules, and polymerizing them. The combination of organic molecules with various functional groups can result in the formation of a variety of organic composites. Particularly, fixing organic molecules on the surface of metal NPs can prevent the aggregation of NPs, allowing a uniform film to be produced through a subsequent spin coating process. When plasmonic metal NPs are evenly distributed on a plasmonic metal film, the interaction of the plasmonic electric fields between the plasmonic metal NPs and the plasmonic metal film can be amplified, leading to enhanced sensitivity. In the context of sensors for the detection of biomolecules, the use of biocomponents to form specific bindings is common. However, if the immobilization layer quality has an impact on repeated measurements, the sensor performance can gradually deteriorate as the fixed biocomponents separate over time. In this case, forming an MIP film using organic composites can enable the development of sensors capable of specific binding even without biocomponents, ensuring long-term stability.

Immunoglobulin G (IgG) is one of the antibodies found in the body fluids of humans and other mammals. IgG binds to specific viruses or bacteria to neutralize their toxicity, and it modulates various immune responses within the immune system.[121] Also, it is essential for regulating immunological reactions. Prior to human trials, studies with mice are frequently carried out to evaluate stability and safety.[80] As a result, there is a growing interest in the sensitive detection of mouse IgG with the increasing demand for mouse IgG. Zhang *et al.* reported the fabrication of an SPR sensor using Ag nanocube (AgNCs)/chitosan composites as sensing materials (Fig. 13(a)).[89] They used organic molecules to produce composites of AgNCs, glutaraldehyde, and chitosan, which were spin-coated onto an Au layer. This composite involved the binding of 3-mercaptopropinic acid (MPA), an organic molecule with thiol functional groups, to AgNCs, forming Ag–S bonds. This process successfully prevented the oxidation of AgNCs. Additionally, the researchers aimed to enhance the sensitivity by spreading AgNCs very uniformly and thinly onto an Au layer, promoting the interaction between the plasmonic electric fields of AgNCs and Au film. Then, they immobilized antibodies for mouse IgG on the surface of the

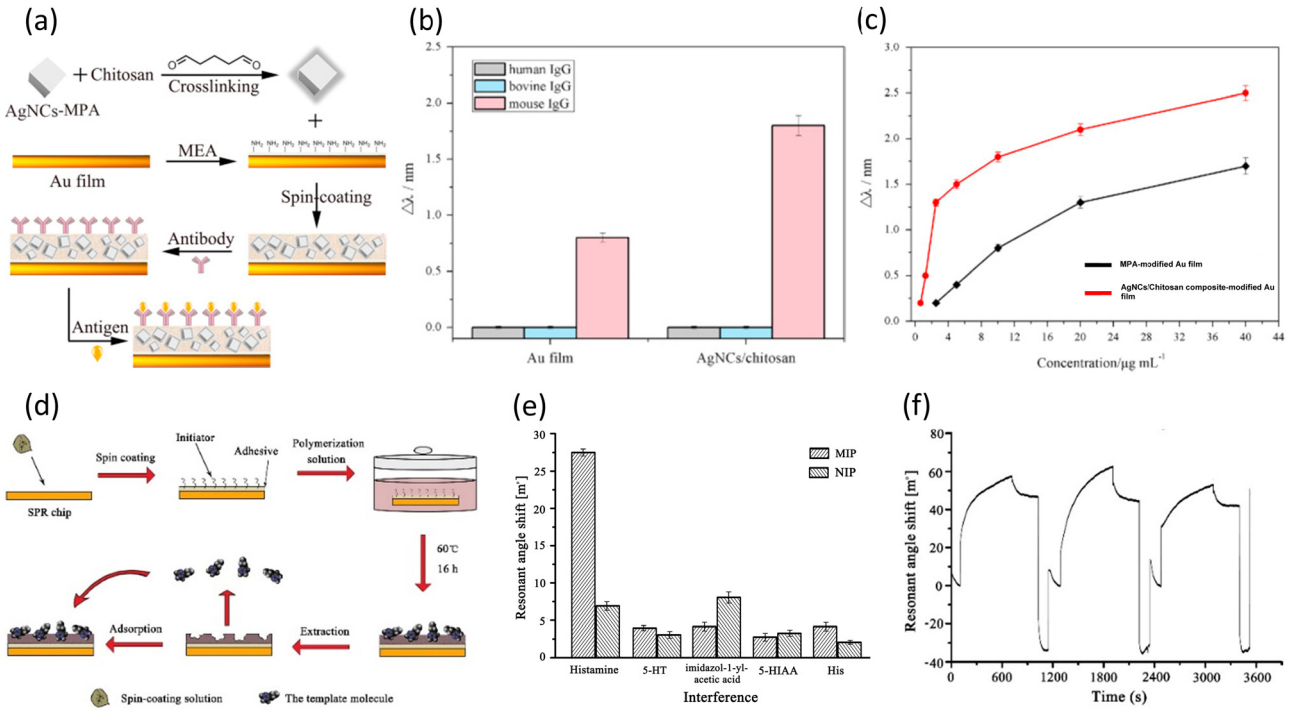

Fig. 13 (a) Schematic for the fabrication of TSNP/chitosan composite-based SPR sensor. (b) Resonance wavelength shifts for interferents on different sensing layers. (c) Resonance wavelength shifts for mouse IgG at different concentrations ranging from 0.6 to 40 μg mL^{-1}. Reproduced with permission from ref. 89 Copyright©2015, Elsevier B.V. (d) Schematic of the fabrication of a histamine-imprinted polymer-based SPR sensor. (e) Resonance angle shifts compared with interferents on MIP and NIP. (f) Real-time and repetitive SPR responses for 500 μg L^{-1} histamine. Reproduced with permission from ref. 90 Copyright© 015, Elsevier B.V.

Open Access Article. Published on 26 February 2025. Downloaded on 2/14/2026 10:12:37 AM. This article is licensed under a Creative Commons Attribution-NonCommercial 3.0 Unported Licence.

composite film by flowing a solution containing the antibodies. Through Schiff alkali reaction with the aldehyde groups of glutaraldehyde, the injected antibodies could be bound. Subsequently, when flowing mouse IgG solution, the immobilized antibodies strongly bind to mouse IgG through antigen–antibody interactions, causing a shift in the resonance wavelength.

Fig. 13(b) compares the resonance wavelength shifts for three different IgGs on both the MPA-modified Au film SPR sensor and the AgNC/chitosan-based SPR sensor after immobilizing the same antibodies on their surfaces. Both sensors showed extremely specific binding to mouse IgG, demonstrating the selectivity of the antibodies utilized in mouse IgG detection. Also, the sensitivity of both sensors to mouse IgG was twice as high in the AgNC/chitosan layer compared to the MPA-modified Au layer. This shows the effectiveness of the proposed AgNC/chitosan layer in enhancing the sensitivity of the SPR sensor, emphasizing its impact on improving the sensitivity in mouse IgG detection. Fig. 13(c) illustrates the resonance wavelength shifts for the AgNC/chitosan composite-based sensor and MPA-modified Au film sensor with respect to the mouse IgG concentration in the range of 0.6 to 40 μg mL^{-1}. Before initiating the detection of mouse IgG, ethanolamine hydrochloride was used to ensure specific binding to the surface of the sensing materials. The AgNCs/chitosan based sensor exhibited a resonance wavelength change of 2.50 nm in the detection range, and the calculated minimum detectable concentration was four-times lower compared to the MPA-modified sensor. It has been shown that uniformly dispersing AgNCs on an Au layer *via* AgNC/chitosan composites improved the plasmonic electric wave of the Au layer, and consequently enhanced the SPR signals.

Histamine, an organic nitrogen compound, serves as a neurotransmitter and actively participates in immune system functions. This small molecule can be found in tissues such as white blood cells and the nervous system. Thus, the accurate detection of histamine is crucial in the fields of medicine, pharmaceuticals, and biotechnology for diagnosing neurological and immunological disorders and developing pharmaceuticals. Jiang *et al.* prepared an MIP film-based SPR sensor for the highly sensitive, selective, and reliable detection of histamine.[90] They used the polymerization of a solution containing histamine and other organic molecules. Subsequently, histamine was removed to form empty sites on the surface (Fig. 13(d)). Histamine could selectively bind to the empty sites during the measurement. Even at a low concentration, histamine could bind to the sites, sufficiently changing the refractive index around the sensing material to generate signals.

The resonance angle shifts were measured for histamine and four interferents to assess the selectivity of the MIP film for histamine using both MIP film-based sensors and non-imprinting polymer (NIP) film-based sensors (Fig. 13(e)). The NIP film-based sensor exhibited resonance angle shifts below 10 m° for all five molecules including histamine, indicating that the NIP film did not sensitively interact with any of the molecules. Alternatively, the MIP film-based sensor showed shifts below 10 m° for four interferents, while histamine showed a significant shift of approximately 27 m°. Considering the concentration differences between the measured histamine (0.1 mg L^{-1}) and interferents (10 mg L^{-1}), it was confirmed that the selectivity and sensitivity of the MIP film for histamine were substantial. The real-time SPR responses for three successive 500 μg L^{-1} histamine detections are shown in Fig. 13(f). After each histamine detection, a regeneration process with 0.1 M HCl solution was conducted to detach histamine from the sensing material. The small differences in resonance angle shifts for each detection confirm the repeatability of this sensor. The resonance angle reached its maximum point within approximately 600 s for each detection, highlighting the real-time detection capability of the proposed sensor. The histamine MIP film-based sensor, as validated by the authors for its selectivity, sensitivity, real-time monitoring, and repeatability, demonstrated the selective binding of histamine to the imprinted sites. Thus, it is anticipated to have a significant impact on researchers and pharmaceutical companies engaged in studies related to histamine.

Various organic composites, such as well-dispersed metal NP layers and MIPs, are being utilized in SPR sensors to enhance their sensitivity and selectivity. Unlike previous technologies for detecting biomolecules, these sensors do not require labels and can be easily measured with simple equipment, eliminating the need for specialized personnel. Moreover, their rapid response time and real-time measurement capabilities make organic composite-based SPR sensors applicable in various fields, including disease diagnosis, pharmaceutical research, and medical studies.

4.3.2 Non-biosensors applications. Selectively detecting chemical molecules with similar structures and characteristics is quite a challenging undertaking. MIP films of organic composites are the most extensively used materials to overcome this challenge. Through the simple polymerization of organic molecules, the target molecules are easily imprinted on the surface of the sensing material. The resulting sensing material shows repeatability through a regeneration process. These materials allow the selective and repeatable detection of molecules in chemical sensors.

Organophosphorus pesticides (OPPs) have been used to kill pests when growing cotton, vegetables, cereals, and other crops. However, even at very low concentrations, OPPs can cause serious neurological diseases in humans and are a major problem for environmental and aquatic organisms because of their comparatively high environmental mobility in water.[122] Consequently, there is a critical need for the rapid and reliable detection of OPPs. However, previously reported methods for detecting OPPs have difficulties such as insufficient selectivity, requirement for labels, and limitation for real-time monitoring. Thus, to overcome these difficulties, research is ongoing to develop approaches for the selective, real-time and label-free detection of OPPs. Shrivastav *et al.* presented an SPR sensor that employed an MIP film to detect the hazardous chemical profenofos, one of the most widely used OPPs.[95] The MIP film functioned by incorporating the target molecule to be detected into the sensing material using organic composites, and then removing it, consequently

 This journal is © The Royal Society of Chemistry 2025

Open Access Article. Published on 26 February 2025. Downloaded on 2/14/2026 10:12:37 AM.
This article is licensed under a Creative Commons Attribution-NonCommercial 3.0 Unported Licence.

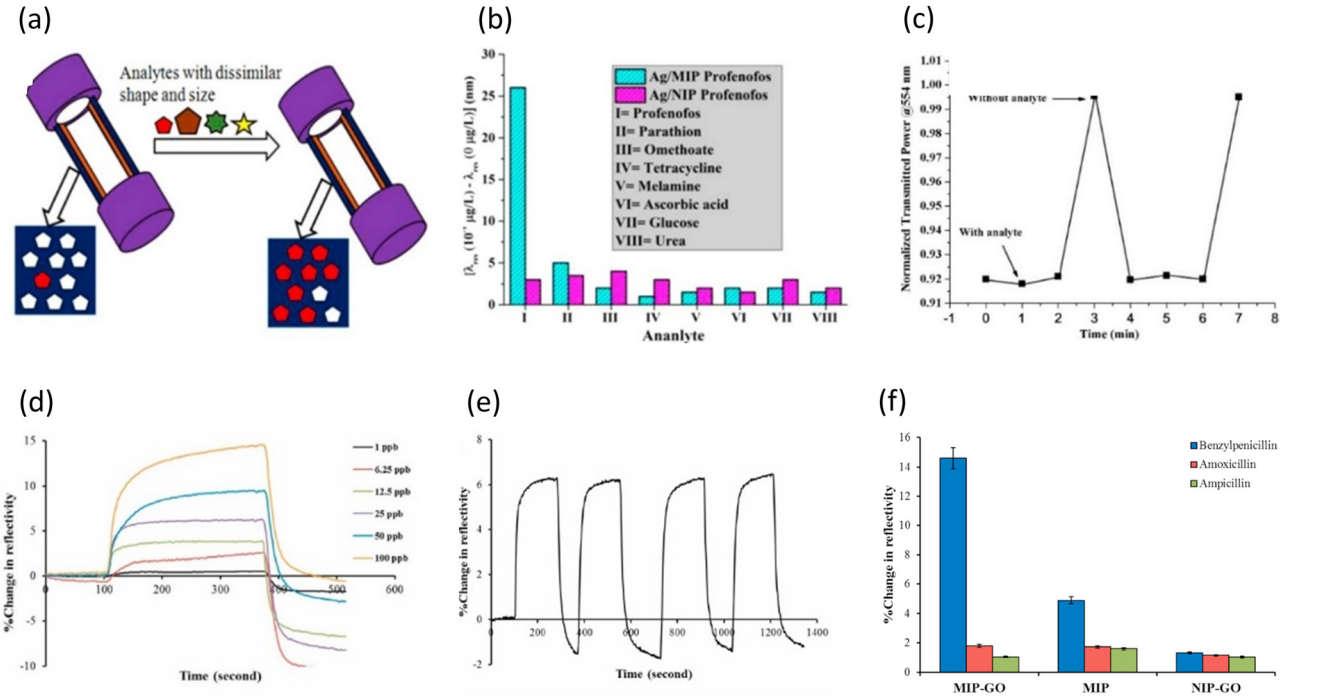

Fig. 14 (a) Schematic of the highly selective and sensitive profenofos-imprinted sensor. (b) Resonance wavelength shifts compared with interferents. (c) Real-time SPR responses for 10^{-4} μg L^{-1} profenofos. Reproduced with permission from ref. 95 Copyright©2015, Elsevier B.V. (d) Real-time SPR responses for benzylpenicillin at different concentrations ranging from 1 to 100 ppb. (e) Repetitive SPR responses for 25 ppb benzylpenicillin. (f) Reflectance changes compared with interferents on different sensing layers. Reproduced with permission from ref. 96 Copyright©2022, Elsevier B.V.

leaving imprinted sites on the surface of the sensing material (Fig. 14(a)). Other molecules cannot bind to the imprinted sites and only profenofos binds to the sites strongly.

As shown in Fig. 14(b), to validate the effectiveness of the MIP film, the authors observed the resonance wavelength shifts of an Ag-based SPR sensor using the MIP film and an Ag-based SPR sensor using an NIP film in response to 0.1 μg L^{-1} profenofos and other interferents. The Ag/NIP sensor without imprinted sites for profenofos showed similar small shifts for profenofos and other interferents. This confirmed that the sensor lacked distinct selectivity and did not respond sensitively to profenofos in the absence of the imprinted sites. Alternatively, the profenofos-imprinted Ag/MIP sensor responded to profenofos intensively, exhibiting a notable shift. It showed a clear difference from seven interferents, indicating its good selectivity. In the Ag-based sensor with MIP film, profenofos can attach firmly and selectively, while interferents have minimal binding on the imprinted sites of the film. The real-time SPR response for 0.0001 μg L^{-1} profenofos is shown in Fig. 14(c). The transmitted intensity at λ = 554 nm was observed with and without profenofos, where profenofos was injected for 2 min, followed by the removal of profenofos for one minute. This process was repeated twice to validate the repeatability of the real-time sensor. Upon the removal of profenofos, there was a significant change in the transmission in about one minute. After one minute of another profenofos injection, the response remained constant and stabilized. These results demonstrated that the sensor could detect profenofos selectively and rapidly in real-time through multiple cycles. The exceptionally fast and selective real-time detection capabilities of the MIP-based SPR sensor reported by Shrivastav's group make it promising for applications in environmental monitoring.

Antibiotics are drugs that support the immune system in both humans and animals by decreasing the activity of pathogens when they are infected. The proper use and disposal of antibiotics can prevent the early invasion of pathogens, allowing the host to overcome the crisis with mild symptoms such as a cold and cough. However, the improper disposal of antibiotics can lead to their discharge into the ecosystem, producing antibiotic-resistant bacteria and causing serious problems.[123] Thus, it is essential to develop sensors that can detect antibiotics that are still present in food and water in real-time. Celik *et al.* reported the fabrication of an SPR sensor with a sensing layer consisting of a GO-based MIP film to detect benzylpenicillin, one of the most widely used β-lactam antibiotics.[96] Through the specific binding of benzylpenicillin in MIP film, the sensor can selectively detect benzylpenicillin. Additionally, GO, a 2D material with excellent electrical and optical properties, was used to amplify the signals from the binding of the target molecule on the imprinted sites. GO possesses a lower work function than Au, and the electron transfer from GO to Au improves the sensitivity of the SPR sensor.[124]

Fig. 14(d) shows the real-time responses of the MIP-GO-based SPR sensor to benzylpenicillin at various concentrations ranging from 1 to 100 ppb. The responses stabilized several

Open Access Article. Published on 26 February 2025. Downloaded on 2/14/2026 10:12:37 AM. This article is licensed under a Creative Commons Attribution-NonCommercial 3.0 Unported Licence.

hundred seconds after the injection of benzylpenicillin, and the sensor exhibited exceptional sensitivity even at ppb levels. Although saturation was achieved within 100 s up to 50 ppb, a concentration of 100 ppb showed a steady increase in response even after 100 s. Overall, as the concentration increased, more binding events occurred, leading to a longer time to be saturated. However, the comparable fast response time up to 50 ppb confirmed the rapid detection of benzylpenicillin in real-time. After that, the repeatability of the MIP-GO-based sensor was measured (Fig. 14(e)). Four successive detections were conducted for 25 ppb benzylpenicillin, and for each detection, 10 mM NaCl was flowed through to desorb benzylpenicillin from the imprinted site. Because there was no additional stabilizing process after each detection, the reflectance changes began with negative values after the initial detection. However, the reflectance changes remained at approximately 6% for the four detections. These constant responses demonstrated that there was no degradation in the binding capacity between MIP and benzylpenicillin even after several adsorption and desorption cycles, thereby confirming the potential of the proposed sensor. Simultaneously, Celik's group conducted comparative experiments using three types of sensing materials and two interferents to demonstrate the improved sensitivity and selectivity achieved through GO and MIP (Fig. 14(f)). By comparing the GO-NIP-based sensor, which lacked imprinted sites and exhibited low responses for all three substances, with the GO-MIP-based sensor, which possessed imprinted sites and showed exceptionally high response only to benzylpenicillin, the selectivity of the MIP film for benzylpenicillin was confirmed. Furthermore, the comparison between the GO-MIP based sensor and the MIP-based sensor revealed that while both sensors exhibited selectivity for benzylpenicillin, the presence of GO resulted in enhanced sensitivity. Celik's group reported that the GO-MIP-based SPR sensor could detect benzylpenicillin rapidly in real-time by amplifying the selective but weak signals from MIP.

Utilizing molecular imprinting films, organic composites become highly effective when there are numerous interferents in the detection environment that may hinder the detection of the target chemical molecules. MIP films can selectively and sensitively capture target molecules due to the presence of imprinted sites. The requirement to immobilize biocomponents for selective detection is removed, lowering the possibility of the detachment of the biocomponents throughout the procedure. This approach can be easily carried out by simply mixing organic molecules and target molecules, and then removing the target molecules. Thus, combining organic composites with SPR sensors, which enable real-time, label-free, and selective detection, holds great potential for applications in environmental monitoring, disease diagnosis, and pharmaceutical research.

5. Practical applications of LSPR and SPR sensors

The significance of the real-world applications of LSPR and SPR sensors stems from their positive impact on many scientific, industrial, and medical areas. In practical applications, these sensors allow the real-time detection of molecular interactions, providing essential insights into biological, chemical, and environmental processes. In healthcare, LSPR and SPR sensors are crucial in drug discovery, medical diagnostics, and biomolecular interaction monitoring, all contributing to advances in precision medicine. Environmental monitoring benefits from the ability to identify pollutants and toxins with high sensitivity. These sensors are used in industrial settings for quality control, process monitoring, and detecting trace contaminants. The real-world application of LSPR and SPR sensors promotes the development of a variety of sectors by providing efficient and dependable instruments for monitoring and analysis, eventually boosting innovation, improving research outcomes, and improving diagnostic and decision-making processes.

Coskun *et al.* presented a microfluidic-based plasmonic biosensing system that combines plasmonic microarrays with dual color lens-free imaging.[125] This system allowed the real-time and multiplexed monitoring of binding events over a large field-of-view (>20 mm^2) in low resource settings. This platform uses an optoelectronic sensor (complementary metal-oxide-semiconductor) to record diffraction patterns of plasmonic nanoapertures at the bottom of a microfluidic channel, as shown in Fig. 15(a)–(c). This allows the controlled delivery of the target solution to surface-functionalized nanosensor arrays. Fig. 15(d) shows that ligand proteins functionalize plasmonic pixels to capture the target proteins. The biosensing device employs a plasmonic nanohole array with excellent light confinement and nanoscale field improvements, resulting in high sensitivity to the surface conditions. Changes in the refractive index near the sensor surface cause a shift in the peak wavelength of the plasmonic mode supported by the nanohole array.

Liu *et al.* presented a flexible, compact dual-channel SPR system.[126] Fig. 15(e) and (h) display a schematic diagram and a photograph and the running interface of the detection system, respectively. Given that all components are attached to the phone case on the back of the smartphone (Fig. 15(f)), the touch-screen interface and display remain unaffected during the detecting process, as shown in Fig. 15(g) and (h). The sensor components and the smartphone can be readily combined into an instrument and dismantled after the measurement.

6. Challenges and future perspectives

LSPR sensors rely on morphological changes in plasmonic metal NPs, while SPR sensors monitor changes in the refractive index around metal films. Although both sensors demonstrate high sensitivity to trace concentrations of analytes, they are vulnerable to environmental interferences. Environmental factors, such as temperature changes and vibrations near the sensors, generate background noise, which is further deteriorated by non-specific adsorption. This undesirable noise increases the LOD, reduces the sensitivity and selectivity, and eventually degrades the overall sensor performance. Therefore,

 This journal is © The Royal Society of Chemistry 2025

Open Access Article. Published on 26 February 2025. Downloaded on 2/14/2026 10:12:37 AM.
This article is licensed under a Creative Commons Attribution-NonCommercial 3.0 Unported Licence.

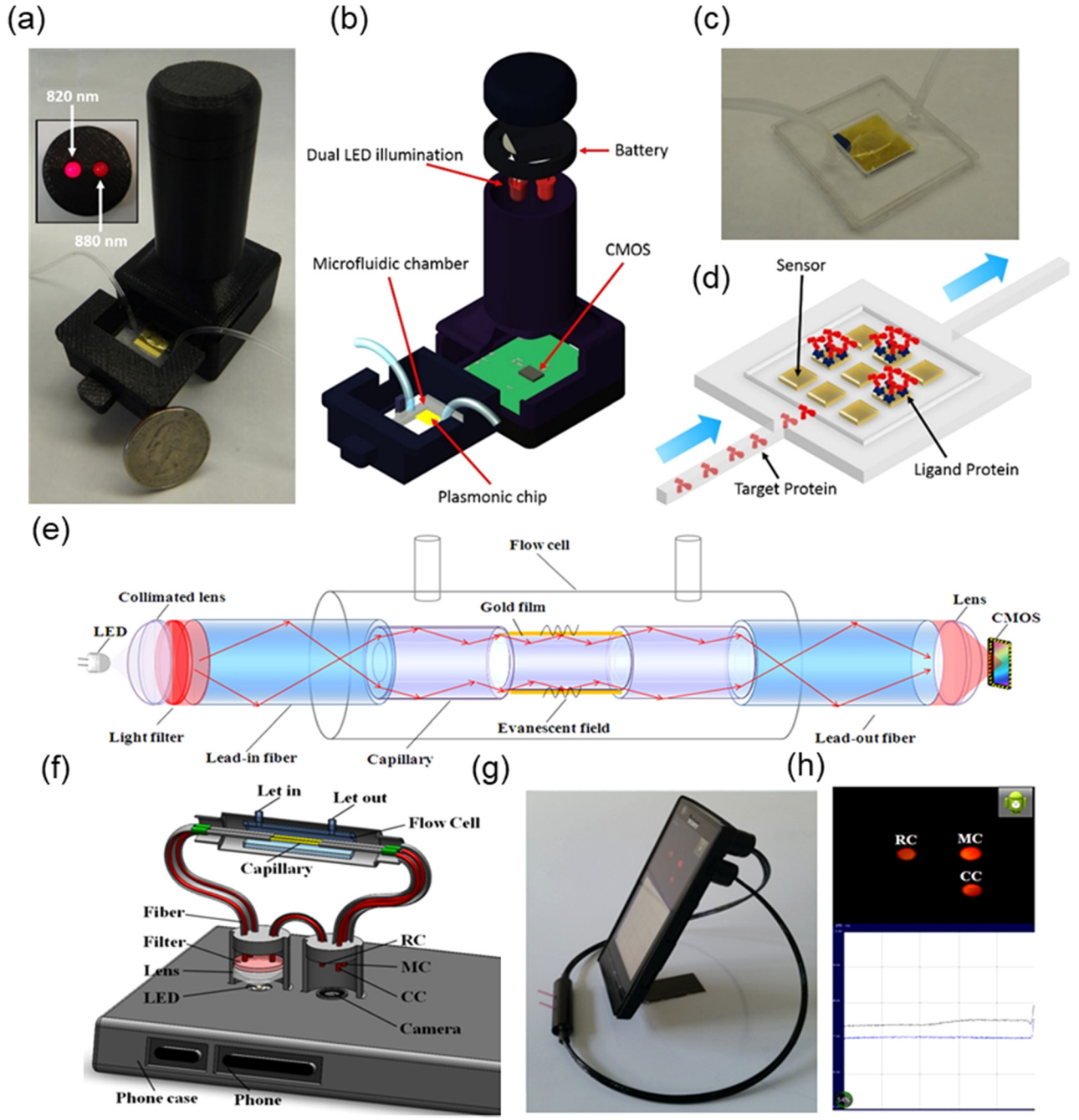

Fig. 15 (a) Photograph and (b) illustration of the LSPR sensing device employing (c) a microfluidic channel. (d) Schematic of the sensing mechanism of microfluidic channel. (b) LSPR peak of SA–Ag composite in an aqueous solution of 1000 ppb of Hg^{2+}. Reproduced with permission from ref. 125 Copyright©2014, Springer Nature. (c) Pb^{2+} sensing mechanism of functionalized AuNPs. Schematic of (e) a smartphone-based SPR sensor and (f) its internal structure. Photograph of (g) SPR sensor installed on a smartphone and (h) the smart phone measurement channel. Reproduced with permission from ref. 126 Copyright©2015, Springer Nature.

addressing these challenges is crucial for improving the reliability and practical applicability of these sensors.

In particular, the synthesis of metal NPs with a uniform size and shape at the nanoscale for LSPR sensors is challenging. Given that their detection mechanism is based on morphological changes, ensuring a uniform distribution of homogeneous metal NPs produces a consistent and strong plasmonic resonance frequency, leading to distinct shifts in the absorption peak and noticeable color changes.[127,128] A variation in the size, shape, or spatial arrangement of the fabricated NP dispersion can reduce the detection accuracy and reproductivity. Thus, advancements in precise synthesis techniques and complementary strategies are essential for reliable detection.

In addition to background noise, SPR sensors are also limited by sensing materials that are either thicker than the effective

Open Access Article. Published on 26 February 2025. Downloaded on 2/14/2026 10:12:37 AM. This article is licensed under a Creative Commons Attribution-NonCommercial 3.0 Unported Licence.

Table 3 General advantages and disadvantages of sensing materials utilized in LSPR and SPR sensor applications

Sensor type	Material type	Advantages	Disadvantages
LSPR sensors	Metal NPs	• Even slight morphological changes in size and shape can significantly affect the plasmonic resonance frequency. • High surface-to-volume ratio maximizes interactions with analytes.	• Difficulty in fabricating metal NPs with uniform size and shape.
	Bimetallic NPs	• Improved stability and sensitivity due to the synergistic effect of each metal. • More flexible tunability in morphology. • Detection with the naked eye through multicolour changes.	• Difficulty in fabricating bimetallic NPs with uniform size and shape.
	MOMs	• Selective binding to analytes *via* surface functionalization of metal NPs. • Reversible detection is possible by capping the surface of metal NPs to prevent their dissociation.	• Poor reproducibility and long-term stability due to degradation of surface functionalization.
SPR sensors	2D materials	• Enhancement of plasmonic waves due to charge transfer from 2D materials to metal films. • Abundant adsorption sites for analytes and anchoring sites for various receptors *via* large specific surface area. • Low damping effect of ultra-thin and uniform surface.	• Formation of undesirable defects during the transfer of 2D materials • High cost for large-area and high-quality production.
	Metal oxides	• Cost-effective and facile synthesis for nanostructures. • Catalytic effect for various chemical and bioanalytes. • Chemical and thermal stability.	• Deterioration of SPR signals due to optical loss in the visible and infrared region.
	Organic composites	• Feasibility of forming uniform films containing metal NPs or bioreceptors. • Highly selective and sensitive detection through MIP films.	• Limitation in controlling the precise thickness at the nanoscale, causing plasmon damping.

detection region or cause optical loss at the resonance wavelength. The evanescent wave, SPP, generated on the metal surface can only penetrate a few hundred nanometers above the metal film.[129] Refractive index changes occurring beyond this detection region are difficult to detect. Moreover, the incident light required to excite a plasmonic wave typically falls within the visible or infrared range. If sensing materials that strongly absorb light in this wavelength range are deposited on the metal film, the intensity of the excited SPP decreases, significantly weakening the SPR signals. Thus, to overcome these problems, depositing ultra-thin sensing materials with suitable optical characteristics is one of the most important considerations in developing SPR sensors.

Despite the challenges faced by LSPR and SPR sensors, ongoing research and development indicate their promising future. Advancements in nanomaterial synthesis, the incorporation of novel materials with plasmonic metals, and progress in optical technology serve as key factors for enhancing the performance and versatility of these sensors. By functionalizing metal surfaces with organic molecules, receptors, and novel materials that selectively bind to analytes without weakening the plasmonic signals, the real-world applications of these sensors can be expanded, increasing their importance. Thus, LSPR and SPR technologies are expected to become valuable candidates in disease diagnostics, drug discovery, and environmental monitoring.

7. Conclusion

LSPR and SPR sensors are plasmonic-based sensors that can precisely detect analytes using optics. LSPR sensors, which detect absorbance through changes in the shape of the sensing material due to interactions, and SPR sensors, which detect changes in refractive index that occur when the sensing material interacts by chemical adsorption, detect very low concentrations of chemicals in real time using cutting-edge sensing materials. Sensing materials for LSPR and SPR sensors play important roles in improving their sensing performance and ability for real-time detection based on rapid response. Table 3, which summarizes the general advantages and disadvantages of each sensing material, provides a clear understanding of how these materials enhance the sensor performance in various applications and the roles they play. As a result, sensing materials such as metal NPs, bimetal NPs, MOMs, 2D materials, metal oxides, and organic composites have been studied, and various structures and compositions have been developed. This material-based research enables lower detection limits and improved real-time sensing capabilities by LSPR and SPR sensors, enabling their use in a wide range of applications requiring real-time sensing, including biomedical diagnostics, environmental, and industrial monitoring. In addition, LSPR and SPR sensors can be miniaturized and easily function using a light source and thus are suitable for application in portable measurement equipment, providing excellent accessibility to measurements that require real-time detection. The combined impact of sensing material improvements and practical applicability presents the significant potential of LSPR and SPR sensors in driving precision and real-time sensing technologies across the scientific, medical, and industrial fields, promising new answers to complex analytical challenges regarding the safe coexistence of chemicals and humanity.

Data availability

Data availability is not applicable to this article as no new data were created or analysed in this study.

 This journal is © The Royal Society of Chemistry 2025

Open Access Article. Published on 26 February 2025. Downloaded on 2/14/2026 10:12:37 AM. This article is licensed under a Creative Commons Attribution-NonCommercial 3.0 Unported Licence.

Conflicts of interest

There are no conflicts to declare.

Acknowledgements

This work was financially supported by the Nano Material Technology Development Program (2022M3H4A1A01011993 & RS-2024-00405016) through the NRF (National Research Foundation of Korea), funded by the Ministry of Science and ICT. Research facilities for this work were provided by the Inter-University Semiconductor Research Center, the Institute of Engineering Research, and Soft Foundry Institute at Seoul National University.

References

1 T. Biswal, S. K. BadJena and D. Pradhan, *Mater. Today: Proc.*, 2020, **30**, 274–282.
2 A. Rahimi and J. M. García, *Nat. Rev. Chem.*, 2017, **1**, 46.
3 M. Harada, *Crit. Rev. Toxicol.*, 1995, **25**, 1–24.
4 A. S. Ayangbenro and O. O. Babalola, *Int. J. Environ. Res. Public Health*, 2017, **14**, 94.
5 S. Lee, X. Bi, R. B. Reed, J. F. Ranville, P. Herckes and P. Westerhoff, *Environ. Sci. Technol.*, 2014, **48**, 10291–10300.
6 W. B. Dunn, D. Broadhurst, P. Begley, E. Zelena, S. Francis-McIntyre, N. Anderson, M. Brown, J. D. Knowles, A. Halsall and J. N. Haselden, *Nat. Protoc.*, 2011, **6**, 1060–1083.
7 N. P. Ivleva, *Chem. Rev.*, 2021, **121**, 11886–11936.
8 M. Rana and V. Mittal, *IEEE Sens. J.*, 2020, **21**, 1187–1207.
9 Q. Pang, D. Lou, S. Li, G. Wang, B. Qiao, S. Dong, L. Ma, C. Gao and Z. Wu, *Adv. Sci.*, 2020, **7**, 1902673.
10 M. Javaid, A. Haleem, R. P. Singh, S. Rab and R. Suman, *Sens Int.*, 2021, **2**, 100110.
11 M. Jayaweera, H. Perera, B. Gunawardana and J. Manatunge, *Environ. Res.*, 2020, **188**, 109819.
12 S. H. Cho, J. M. Suh, T. H. Eom, T. Kim and H. W. Jang, *Electron. Mater. Lett.*, 2021, **17**, 1–17.
13 S. H. Cho, M.-J. Choi, B. Koo, J. Kim, T. H. Lee, J. M. Suh, T. H. Eom, S. Y. Park, T. Kim and W. Jung, *Sens. Actuators, B*, 2024, **403**, 135137.
14 S. Hwan Cho, J. Min Suh, B. Jeong, T. Hyung Lee, K. Soon Choi, T. Hoon Eom, T. Kim and H. Won Jang, *Chem. Eng. J.*, 2022, **446**, 136862.
15 C. W. Lee, J. M. Suh, S. Choi, S. E. Jun, T. H. Lee, J. W. Yang, S. A. Lee, B. R. Lee, D. Yoo, S. Y. Kim, D. S. Kim and H. W. Jang, *npj 2D Mater. Appl.*, 2021, **5**, 1–13.
16 A. Kumar and R. Prajesh, *Sens. Actuators, A*, 2022, **339**, 113498.
17 Q. Duan, Y. Liu, S. Chang, H. Chen and J. Chen, *Sensors*, 2021, **21**, 5262.
18 J. Homola, S. S. Yee and G. Gauglitz, *Sens. Actuators, B*, 1999, **54**, 3–15.
19 J. N. Anker, W. P. Hall, O. Lyandres, N. C. Shah, J. Zhao and R. P. Van Duyne, *Nat. Mater.*, 2008, **7**, 442–453.
20 J. Homola, *Chem. Rev.*, 2008, **108**, 462–493.
21 K. M. Mayer and J. H. Hafner, *Chem. Rev.*, 2011, **111**, 3828–3857.
22 J.-F. Masson, *Analyst*, 2020, **145**, 3776–3800.
23 G. Simone, *Crit. Rev. Anal. Chem.*, 2024, **54**, 2183–2208.
24 J. Homola, *Anal. Bioanal. Chem.*, 2003, **377**, 528–539.
25 X. Zhang, Z. Li, W. Yan, A. Li, F. Zhang, X. Li, M. Lu and W. Peng, *Talanta*, 2024, **269**, 125440.
26 S. Long, J. Cao, Y. Wang, S. Gao, N. Xu, J. Gao and W. Wan, *Sens. Actuators Rep.*, 2020, **2**, 100016.
27 G. Mie, *Ann. Phys.*, 1908, **330**, 377–445.
28 K. Matsubara, S. Kawata and S. Minami, *Appl. Spectrosc.*, 1988, **42**, 1375–1379.
29 K. Matsubara, S. Kawata and S. Minami, *Opt. Lett.*, 1990, **15**, 75–77.
30 G. Cappi, F. M. Spiga, Y. Moncada, A. Ferretti, M. Beyeler, M. Bianchessi, L. Decosterd, T. Buclin and C. Guiducci, *Anal. Chem.*, 2015, **87**, 5278–5285.
31 V. G. Kravets, F. Schedin, A. V. Kabashin and A. N. Grigorenko, *Opt. Lett.*, 2010, **35**, 956–958.
32 M. Pirzada and Z. Altintas, *Micromachines*, 2020, **11**, 356.
33 K. M. Mayer and J. H. Hafner, *Chem. Rev.*, 2011, **111**, 3828–3857.
34 P. Englebienne, A. Van Hoonacker and M. Verhas, *J. Spectrosc.*, 2003, **17**, 255–273.
35 J. Chen, A. A. Jackson, V. M. Rotello and S. R. Nugen, *Small*, 2016, **12**, 2469–2475.
36 X. Liu, J. Wang, Y. Wang, C. Huang, Z. Wang and L. Liu, *ACS Omega*, 2021, **6**, 23630–23635.
37 A. Amirjani, M. Bagheri, M. Heydari and S. Hesaraki, *Nanotechnology*, 2016, **27**, 375503.
38 J. Lerdsri, W. Chananchana, J. Upan, T. Sridara and J. Jakmunee, *Sens. Actuators, B*, 2020, **320**, 128356.
39 Q. Zhu, T. Li, Y. Ma, Z. Wang, J. Huang, R. Liu and Y. Gu, *RSC Adv.*, 2017, **7**, 19250–19256.
40 S. Rasheed, N. Ahmad, M. A. ul Haq, W. Ahmad and D. Hussain, *J. Ind. Eng. Chem.*, 2023, **128**, 450–458.
41 Z. Zhang, Z. Chen, C. Qu and L. Chen, *Langmuir*, 2014, **30**, 3625–3630.
42 P. Huang, B. Liu, W. Jin, F. Wu and Y. Wan, *J. Nanopart. Res.*, 2016, **18**, 1–9.
43 K. Shrivas, R. Shankar and K. Dewangan, *Sens. Actuators, B*, 2015, **220**, 1376–1383.
44 S. Chen, J. Tang, Y. Kuang, L. Fu, F. Ma, Y. Yang, G. Chen and Y. Long, *Sens. Actuators, B*, 2015, **221**, 1182–1187.
45 H. He, X. Xu, H. Wu and Y. Jin, *Adv. Mater.*, 2012, **24**, 1736–1740.
46 Y. Wang, P. Zhang, W. Fu and Y. Zhao, *Biosens. Bioelectron.*, 2018, **122**, 183–188.
47 Y. Wang, P. Zhang, X. Mao, W. Fu and C. Liu, *Sens. Actuators, B*, 2016, **231**, 95–101.
48 Y. Wang, Y. Zeng, W. Fu, P. Zhang, L. Li, C. Ye, L. Yu, X. Zhu and S. Zhao, *Anal. Chim. Acta*, 2018, **1002**, 97–104.
49 H. Lee, H. K. Sung, C. Park and Y. Kim, *J. Ind. Eng. Chem.*, 2017, **48**, 235–241.
50 I. Darmadi, S. Z. Khairunnisa, D. Tomecek and C. Langhammer, *ACS Appl. Nano Mater.*, 2021, **4**, 8716–8722.

Open Access Article. Published on 26 February 2025. Downloaded on 2/14/2026 10:12:37 AM. This article is licensed under a Creative Commons Attribution-NonCommercial 3.0 Unported Licence.

51 X. Li, X. Lin, S. Lin, X. Sun, D. Gao, B. Liu, H. Zhao, J. Zhang, S. Cong and L. Wang, *ACS Appl. Nano Mater.*, 2019, **2**, 3161–3168.
52 J.-K. Chen, S.-M. Zhao, J. Zhu, J.-J. Li and J.-W. Zhao, *J. Alloys Compd.*, 2020, **828**, 154392.
53 Z. Qiu, Y. Xue, J. Li, Y. Zhang, X. Liang, C. Wen, H. Gong and J. Zeng, *Chin. Chem. Lett.*, 2021, **32**, 2807–2811.
54 S. Li, T. Wei, M. Tang, F. Chai, F. Qu and C. Wang, *Sens. Actuators, B*, 2018, **255**, 1471–1481.
55 Y. Xia, J. Ye, K. Tan, J. Wang and G. Yang, *Anal. Chem.*, 2013, **85**, 6241–6247.
56 Z. Karimzadeh, A. Jouyban, M. Khoubnasabjafari, A. Gharakhani and E. Rahimpour, *Plasmonics*, 2022, **17**, 1999–2008.
57 H.-M. Kim, W.-J. Kim, K.-O. Kim, J.-H. Park and S.-K. Lee, *J. Alloys Compd.*, 2021, **884**, 161140.
58 D. Sahu, N. Sarkar, G. Sahoo, P. Mohapatra and S. K. Swain, *Sens. Actuators, B*, 2017, **246**, 96–107.
59 A. R. Ferhan, L. Guo, X. Zhou, P. Chen, S. Hong and D.-H. Kim, *Anal. Chem.*, 2013, **85**, 4094–4099.
60 S. S. Dandu, D. J. Joshi, T. J. Park and S. K. Kailasa, *Appl. Spectrosc.*, 2023, **77**, 360–370.
61 I. E. Paul, A. Rajeshwari, T. C. Prathna, A. M. Raichur, N. Chandrasekaran and A. Mukherjee, *Anal. Methods*, 2015, **7**, 1453–1462.
62 J. Song, F. Wu, Y. Wan and L. Ma, *Food Control*, 2015, **50**, 356–361.
63 I. Onyido, A. R. Norris and E. Buncel, *Chem. Rev.*, 2004, **104**, 5911–5930.
64 F. J. Gifford, R. M. Gifford, M. Eddleston and N. Dhaun, *Kidney Int. Rep.*, 2017, **2**, 282–292.
65 M. Fisser, R. A. Badcock, P. D. Teal and A. Hunze, *Sens. Actuators, B*, 2018, **259**, 10–19.
66 S. H. Cho, J. M. Suh, B. Jeong, T. H. Lee, K. S. Choi, T. H. Eom, T. Kim and H. W. Jang, *Chem. Eng. J.*, 2022, **446**, 136862.
67 C. Wadell, S. Syrenova and C. Langhammer, *ACS Nano*, 2014, **8**, 11925–11940.
68 L. Boon-Brett, J. Bousek, G. Black, P. Moretto, P. Castello, T. Hübert and U. Banach, *Int. J. Hydrogen Energy*, 2010, **35**, 373–384.
69 H. Gao, M. Liu, Z. Zhao, C. Yang, L. Zhu, Y. Cai, Y. Yang and Z. Hu, *ACS Appl. Mater. Interfaces*, 2020, **12**, 9693–9700.
70 S. Chang, L. Liu, C. Mu, F. Wen, J. Xiang, K. Zhai, B. Wang, L. Wu, A. Nie and Y. Shu, *J. Colloid Interface Sci.*, 2023, **651**, 938–947.
71 J. Feng, J. Gao, W. Yang, Y. Li, J. Shi, C. Liu, M. Jiang and S. Jiang, *ACS Appl. Nano Mater.*, 2023, **6**, 12775–12783.
72 P. Thawany, A. Khanna, U. K. Tiwari and A. Deep, *Sci. Rep.*, 2023, **13**, 5297.
73 Q. Wu, N. Li, Y. Wang, Y. Xu, S. Wei, J. Wu, G. Jia, X. Fang, F. Chen and X. Cui, *Biosens. Bioelectron.*, 2019, **144**, 111697.
74 Y. Wang, Z. Mao, Q. Chen, K. Koh, X. Hu and H. Chen, *Biosens. Bioelectron.*, 2022, **201**, 113954.
75 J. Ma, B. Lu, P. Zhang, D. Li and K. Xu, *Sens. Actuators, A*, 2023, **353**, 114227.
76 T. Xue, W. Liang, Y. Li, Y. Sun, Y. Xiang, Y. Zhang, Z. Dai, Y. Duo, L. Wu and K. Qi, *Nat. Commun.*, 2019, **10**, 28.
77 S. H. Cho, J. M. Suh, W. Kim, J. Kim, Y. J. Kim, T. H. Lee, J. Y. Kim, J. Sim, S. W. Choi and B. H. Hong, *Energy Environ. Mater.*, 2025, **8**(1), e12801.
78 S. Gan, B. Ruan, Y. Xiang and X. Dai, *IEEE Sens. J.*, 2020, **21**, 347–352.
79 R. Chen, C. Guo, G. Lan, P. Luo, J. Yi and W. Wei, *Biosens. Bioelectron.*, 2023, 115469.
80 R. Kant, R. Tabassum and B. D. Gupta, *Biosens. Bioelectron.*, 2018, **99**, 637–645.
81 T. O. C. Rahayu, N. L. W. Septiani, G. Gumilar, D. R. Adhika and B. Yuliarto, *IEEE Sens. J.*, 2021, **21**, 19959–19966.
82 B. Karki, Y. Trabelsi, A. Pal, S. A. Taya and R. B. Yadav, *Opt. Mater.*, 2024, **147**, 114555.
83 G. Kaur, A. Paliwal, M. Tomar and V. Gupta, *Biosens. Bioelectron.*, 2016, **78**, 106–110.
84 R. Kant, *Microchim. Acta*, 2020, **187**, 1–11.
85 A. Paliwal, A. Sharma, M. Tomar and V. Gupta, *Sens. Actuators, B*, 2015, **216**, 497–503.
86 S. K. Mishra, S. Rani and B. D. Gupta, *Sens. Actuators, B*, 2014, **195**, 215–222.
87 A. Paliwal, A. Sharma, M. Tomar and V. Gupta, *Sens. Actuators, B*, 2017, **250**, 679–685.
88 Y. Mustapha Kamil, S. H. Al-Rekabi, M. H. Abu Bakar, Y. W. Fen, H. A. Mohammed, N. H. Mohamed Halip, M. T. Alresheedi and M. A. Mahdi, *Photonic Sens.*, 2022, **12**, 220306.
89 D. Zhang, Y. Sun, Q. Wu, P. Ma, H. Zhang, Y. Wang and D. Song, *Talanta*, 2016, **146**, 364–368.
90 S. Jiang, Y. Peng, B. Ning, J. Bai, Y. Liu, N. Zhang and Z. Gao, *Sens. Actuators, B*, 2015, **221**, 15–21.
91 J. Zhang, Y. Sun, H. Zhang, B. Xu, H. Zhang and D. Song, *Anal. Chim. Acta*, 2013, **769**, 114–120.
92 X. Xu, Y. Zhang, B. Wang, L. Luo, Z. Xu and X. Tian, *RSC Adv.*, 2018, **8**, 32538–32544.
93 S. Nangare and P. Patil, *Int. J. Biol. Macromol.*, 2022, **214**, 568–582.
94 A. Baliyan, P. Bhatia, B. D. Gupta, E. K. Sharma, A. Kumari and R. Gupta, *Sens. Actuators, B*, 2013, **188**, 917–922.
95 A. M. Shrivastav, S. P. Usha and B. D. Gupta, *Biosens. Bioelectron.*, 2016, **79**, 150–157.
96 O. Çelik, Y. Saylan, I. Göktürk, F. Yılmaz and A. Denizli, *Talanta*, 2023, **253**, 123939.
97 N. Atar, T. Eren, M. L. Yola and S. Wang, *Sens. Actuators, B*, 2015, **216**, 638–644.
98 R. Verma and B. D. Gupta, *Food Chem.*, 2015, **166**, 568–575.
99 K. Chung, J. S. Lee, E. Kim, K. Lee, K. Kim, J. Lee, D. Kim, S. O. Kim, S. Jeon and H. Park, *Adv. Mater. Interfaces*, 2018, **5**, 1800433.
100 S. H. Choi, Y. L. Kim and K. M. Byun, *Opt. Express*, 2011, **19**, 458–466.
101 G. M. Varghese, R. John, A. Manesh, R. Karthik and O. C. Abraham, *Indian J. Med. Res.*, 2020, **151**, 401.

 This journal is © The Royal Society of Chemistry 2025

Open Access Article. Published on 26 February 2025. Downloaded on 2/14/2026 10:12:37 AM.
This article is licensed under a Creative Commons Attribution-NonCommercial 3.0 Unported Licence.

102 T. Ohmi, S. Sudoh and H. Mishima, *IEEE Trans. Semicond. Manuf.*, 1994, **7**, 440–446.
103 D. Shin, H. R. Kim and B. H. Hong, *Nanoscale Adv.*, 2021, **3**, 1404–1412.
104 A. Das, S. Pisana, B. Chakraborty, S. Piscanec, S. K. Saha, U. V. Waghmare, K. S. Novoselov, H. R. Krishnamurthy, A. K. Geim, A. C. Ferrari and A. K. Sood, *Nat. Nanotechnol.*, 2008, **3**, 210–215.
105 C. W. Lee, S. E. Jun, S. J. Kim, T. H. Lee, S. A. Lee, J. W. Yang, J. H. Cho, S. Choi, C. Kim, S. Y. Kim and H. W. Jang, *InfoMat*, 2023, **5**, e12427.
106 C. Lin and S. Chen, *Opt. Commun.*, 2019, **445**, 155–160.
107 A. Salinas-Castillo, I. Pastor, R. Mallavia and C. R. Mateo, *Biosens. Bioelectron.*, 2008, **24**, 1053–1056.
108 A. Bornø, L. Foged and G. van Hall, *J. Mass Spectrom.*, 2014, **49**, 980–988.
109 P. Kalimuthu, S. Leimkühler and P. V. Bernhardt, *Anal. Chem.*, 2012, **84**, 10359–10365.
110 J. K. Kirk and J. Stegner, *J. Diabetes Sci. Technol.*, 2010, **4**, 435–439.
111 R. M. Anjana, R. Pradeepa, M. Deepa, M. Datta, V. Sudha, R. Unnikrishnan, A. Bhansali, S. R. Joshi, P. P. Joshi and C. S. Yajnik, *Diabetologia*, 2011, **54**, 3022–3027.
112 R. D. Janine Freeman and M. P. H. Lynne Lyons, *Diabetes spectrum*, 2008, **21**, 134.
113 M. Flockhart and F. J. Larsen, *Sports Med.*, 2023, 1–9.
114 T. H. Eom, S. H. Cho, J. M. Suh, T. Kim, J. W. Yang, T. H. Lee, S. E. Jun, S. J. Kim, J. Lee, S. H. Hong and H. W. Jang, *Small*, 2022, **18**, 1–12.
115 D. Cho, J. M. Suh, S. Nam, S. Y. Park, M. Park, T. H. Lee, K. S. Choi, J. Lee, C. Ahn and H. W. Jang, *Adv. Sci.*, 2021, **8**, 2001883.
116 Y.-S. Shim and H. W. Jang, *J. Sens. Sci. Technol.*, 2016, **25**, 178–183.
117 G. Weinmayr, E. Romeo, M. de Sario, S. K. Weiland and F. Forastiere, *Environ. Health Perspect.*, 2010, **118**, 449–457.
118 Z. Xu, W. Shi, C. Yang, J. Xu, H. Liu, J. Xu and B. Zhu, *Luminescence*, 2020, **35**, 299–304.
119 T. H. Eom, S. H. Cho, J. M. Suh, T. Kim, T. H. Lee, S. E. Jun, J. W. Yang, J. Lee, S. H. Hong and H. W. Jang, *J. Mater. Chem. A*, 2021, **9**, 11168–11178.
120 C. Müller, T. Nirmaier, A. Rügemer and M. V. Schickfus, *Sens. Actuators, B*, 2000, **68**, 69–73.
121 K. Baker, T. Rath, W. I. Lencer, E. Fiebiger and R. S. Blumberg, *Cell. Mol. Life Sci.*, 2013, **70**, 1319–1334.
122 K. Rekha, M. D. Gouda, M. S. Thakur and N. G. Karanth, *Biosens. Bioelectron.*, 2000, **15**, 499–502.
123 F. Baquero, J.-L. Martínez and R. Cantón, *Curr. Opin. Biotechnol*, 2008, **19**, 260–265.
124 S. Ji, B. K. Min, S. K. Kim, S. Myung, M. Kang, H.-S. Shin, W. Song, J. Heo, J. Lim and K.-S. An, *Appl. Surf. Sci.*, 2017, **419**, 252–258.
125 A. F. Coskun, A. E. Cetin, B. C. Galarreta, D. A. Alvarez, H. Altug and A. Ozcan, *Sci. Rep.*, 2014, **4**, 6789.
126 Y. Liu, Q. Liu, S. Chen, F. Cheng, H. Wang and W. Peng, *Sci. Rep.*, 2015, **5**, 12864.
127 A. G. M. da Silva, T. S. Rodrigues, J. Wang, L. K. Yamada, T. V. Alves, F. R. Ornellas, R. A. Ando and P. H. C. Camargo, *Langmuir*, 2015, **31**, 10272–10278.
128 A. D. Chowdhury, F. Nasrin, R. Gangopadhyay, A. B. Ganganboina, K. Takemura, I. Kozaki, H. Honda, T. Hara, F. Abe, S. Park, T. Suzuki and E. Y. Park, *Biosens. Bioelectron.*, 2020, **170**, 112657.
129 S. J. Yoon and D. Kim, *J. Opt. Soc. Am. A*, 2007, **24**, 2543–2549.